2022

Another Shipment of Six Short-Period Giant Planets from TESS

Joseph E. Rodriguez

Samuel N. Quinn

Andrew Vanderburg

George Zhou

Jason D. Eastman

See next page for additional authors

Authors

Joseph E. Rodriguez, Samuel N. Quinn, Andrew Vanderburg, George Zhou, Jason D. Eastman, Erica Thygesen, Bryson Cale, David R. Ciardi, Phillip A. Reed, and Ryan J. Oelkers

MNRAS 000, 1–20 (2022) Preprint 13 May 2022 Compiled using MNRAS LaTeX style file v3.0

Another Shipment of Six Short-Period Giant Planets from *TESS*

Joseph E. Rodriguez,[1⋆] Samuel N. Quinn,[2] Andrew Vanderburg,[3] George Zhou,[4] Jason D. Eastman,[2] Erica Thygesen,[1] Bryson Cale,[5] David R. Ciardi,[5] Phillip A. Reed,[6] Ryan J. Oelkers,[7,8,9] Karen A. Collins,[2] Allyson Bieryla,[2] David W. Latham,[2] B. Scott Gaudi,[10] Coel Hellier,[11] Kirill Sokolovsky,[1] Jack Schulte,[1] Gregor Srdoc,[12] John Kielkopf,[13] Ferran Grau Horta,[14] Bob Massey,[15] Phil Evans,[16] Denise C. Stephens,[17] Kim K. McLeod,[18] Nikita Chazov,[19] Vadim Krushinsky,[19] Mourad Ghachoui,[20,21] Boris S. Safonov,[22] Cayla M. Dedrick,[23,24] Dennis Conti,[25] Didier Laloum,[25] Steven Giacalone,[26] Carl Ziegler,[27] Pere Guerra Serra,[28] Ramon Naves Nogues,[29] Felipe Murgas,[30,31] Edward J. Michaels,[32] George R. Ricker,[3] Roland K. Vanderspek,[3] Joshua N. Winn,[33] Jon M. Jenkins,[34] Brett Addison,[4] Owen Alfaro,[35] D. R. Anderson,[13,36] Elias Aydi,[1] Timothy Bedding,[37] Alexander A. Belinski,[22] Zouhair Benkhaldoun,[20] Perry Berlind,[2] Cullen H. Blake,[38] Michael J. Bowen,[35] Brendan P. Bowler,[39] Andrew W. Boyle,[5] Dalton Branson,[40] César Briceño,[41] Michael L. Calkins,[2] Emma Campbell,[18] Laura Chomiuk,[1,] Kevin I. Collins,[35] Matthew A. Co Ahmed Daassou,[43] Courtney D. Dressing,[26] Gilbert A. Esquerdo,[2] Dax L. Feliz,[44] William Fong,[3] Tianjun Gan,[45] Holden Gill,[26] Maria V. Goliguzova,[22] Jarrod Hansen,[17] Eric G. Hintz,[17] Jonathan Horner,[4] Chelsea X. Huang,[4] David J. James,[46] Jacob S. Jensen,[17] Samson A. Johnson,[10] Stephen R. Kane,[47] Khalid Barkaoui,[21,48,30] Myung-Jin Kim,[49] Kingsley Kim,[50] Rudolf B. Kuhn,[51,52] Nicholas Law,[53] Pablo Lewin,[54] Hui-Gen Liu,[55] Michael B. Lund,[5] Andrew W. Mann,[53] Nate McCrady,[40] Matthew W. Mengel,[4] Jessica Mink,[2] Lauren G. Murphy,[6] Norio Narita,[30,56,57] Patrick Newman,[38] Jack Okumura,[4] Hugh P. Osborn,[3,58] Martin Paegert,[2] Enric Palle,[30,31] Joshua Pepper,[59] Peter Plavchan,[35] Alexander A. Popov,[19] Markus Rabus,[60] Jessica Ranshaw,[1] Jennifer A. Rodriguez,[1] Dong-Goo Roh,[56] Michael A. Reefe,[3] Arjun B. Savel,[61] Richard P. Schwarz,[62] Avi Shporer,[3] Robert J. Siverd,[63] David H. Sliski,[38] Keivan G. Stassun,[44,64] Daniel J. Stevens,[23,24] Abderahmane Soubkiou,[20,65,66] Eric B. Ting,[34] C.G. Tinney,[67] Noah Vowell,[1] R. G. West,[36,68] Maurice L. Wilson,[2] Robert A. Wittenmyer,[4] Justin M. Wittrock,[35] Jason T. Wright,[23,24,69] Hui Zhang,[70] and Evan Zobel[1]
Affiliations are listed at the end of the paper

Accepted XXX. Received YYY; in original form ZZZ

ABSTRACT

We present the discovery and characterization of six short-period, transiting giant planets from NASA's *Transiting Exoplanet Survey Satellite (TESS)* — TOI-1811 (TIC 376524552), TOI-2025 (TIC 394050135), TOI-2145 (TIC 88992642), TOI-2152 (TIC 395393265), TOI-2154 (TIC 428787891), & TOI-2497 (TIC 97568467). All six planets orbit bright host stars ($8.9 < G < 11.8$, $7.7 < K < 10.1$). Using a combination of time-series photometric and spectroscopic follow-up observations from the *TESS* Follow-up Observing Program (TFOP) Working Group, we have determined that the planets are Jovian-sized (R_P = 1.00-1.45 R_J), have masses ranging from 0.92 to 5.35 M_J, and orbit F, G, and K stars ($4753 \leq T_{eff} \leq 7360$ K). We detect a significant orbital eccentricity for the three longest-period systems in our sample: TOI-2025 b (P = 8.872 days, $e = 0.220 \pm 0.053$), TOI-2145 b (P = 10.261 days, $e = 0.182^{+0.039}_{-0.049}$), and TOI-2497 b (P = 10.656 days, $e = 0.196^{+0.059}_{-0.053}$). TOI-2145 b and TOI-2497 b both orbit subgiant host stars ($3.8 < \log g < 4.0$), but these planets show no sign of inflation despite very high levels of irradiation. The lack of inflation may be explained by the high mass of the planets; $5.35^{+0.32}_{-0.35}$ M_J (TOI-2145 b) and 5.21 ± 0.52 M_J (TOI-2497 b). These six new discoveries contribute to the larger community effort to use *TESS* to create a magnitude-complete, self-consistent sample of giant planets with well-determined parameters for future detailed studies.

Key words: Exoplanets – Stars – transits

1 INTRODUCTION

While NASA's *Transiting Exoplanet Survey Satellite* (*TESS*) mission continues to discover a wealth of new small planets, it is also discovering many transiting hot and warm Jupiters, complementing the prior work of ground-based transit surveys (Pollacco et al. 2006; Pepper et al. 2007; Bakos et al. 2013) and space-based surveys like NASA's *Kepler* and *K2* missions (Borucki et al. 2010; Howell et al. 2014) and ESA's CoRoT satellite (Auvergne et al. 2009). These surveys discovered hundreds of hot Jupiters and established that they are rare (<1%). Using observations from *Kepler*, three different occurrence rates of hot Jupiters have been measured: 0.43±0.05% (Fressin et al. 2013), $0.57^{+0.14}_{-0.12}$% (Petigura et al. 2018), and $0.43^{+0.07}_{-0.06}$% (Masuda & Winn 2017). However, radial velocity (RV) surveys have measured the occurrence rate to be a bit higher: 1.5±0.6% (Cumming et al. 2008) and 1.2±0.4% (Wright et al. 2012), with the difference in occurrence rates possibly due to the removal of spectroscopic binaries (SB2 that show two sets of lines and short-period SB1s where only one set of lines is detected but with a large RV offset consistent with a stellar companion) in the RV surveys (Moe & Kratter 2021). Since the surveys have different target selection criteria, these results suggest that the occurrence rates depend on the properties of the host star (mass, multiplicity, age, etc). Zhou et al. (2019) gave a first glimpse into the occurrence rate from the primary mission of NASA's *TESS* (Ricker et al. 2015)), measuring an occurrence rate of 0.41±0.10%, consistent with results from the *Kepler* mission. Zhou et al. (2019) used *TESS* data to measure occurrence rates as a function of spectral type and found it to be 0.71 ± 0.31% for G stars, 0.43 ± 0.15% for F stars, and 0.26 ± 0.11% for A stars.

As a result of its observing strategy and photometric precision, *TESS* should be nearly complete for discovering transiting hot Jupiters (P<10 days, $TESS_{Mag} < 10$, Zhou et al. 2019), providing the community with the opportunity to create a homogeneous, magnitude-complete population of giant planet parameters. Unfortunately, most ground-based surveys struggled to discover transiting planets with periods above ∼5 days due to their poor duty cycle (Gaudi et al. 2005). However, much work remains as recent results suggest that the current sample of known hot Jupiters is only 75% complete for stars brighter than Gaia magnitude (Gaia Collaboration et al. 2018) G≤10.5, 50% for G≤12, and 36% at G≤12.5 (Yee et al. 2021). Fortunately, coordinated RV efforts within the *TESS* Follow-up Observing Program (TFOP) are helping to extend this sample to G <12.5. As we continue to confirm new hot Jupiters from *TESS*, we will gain insight into some of the key questions about their formation and evolutionary pathways (see reviews, e.g., Dawson & Johnson 2018; Fortney et al. 2021).

Here we present the discovery and characterization of six new hot and warm giant planets from NASA's *TESS* mission. These six targets were selected for follow up confirmation as part of a large effort to discover and characterize transiting hot and warm Jupiters with the goal of creating a magnitude-complete sample of giant planets with measured eccentricities (Rodriguez et al. 2019, 2021; Ikwut-Ukwa et al. 2022). These discoveries, combined with other large scale efforts to use *TESS* to confirm and characterize giant planets (Nielsen et al. 2019; Brahm et al. 2020; Addison et al. 2021; Grunblatt et al. 2022, Yee et al. submitted), should lead to a magnitude-complete sample of hot Jupiters for future population studies. During the preparation of this paper, we became aware of another effort to announce the discovery of TOI-2025 b (Knudstrup et al. 2022). Future efforts should combine all observations of TOI-2025 b presented in both discovery papers. All results presented here on TOI-2025 were independently determined, and all communication between both groups was related to coordinating submissions. In §2 we present the *TESS* and follow-up observations. We review our global analysis using `EXOFASTv2` (Eastman et al. 2019) in §3 and discuss our results in §4, specifically the impact *TESS* is having on our understanding of hot Jupiters. Our conclusions for this work are summarized in §5.

2 OBSERVATIONS AND ARCHIVAL DATA

We used a series of photometric and spectroscopic observations to rule out false positive scenarios, confirm planet candidates as bona fide planets, and measure key parameters such as orbital eccentricity and the planet's mass. All observations presented here were coordinated through the *TESS* Follow-up Observing Program (TFOP) Working Groups. The literature values for previously measured parameters of these stars are listed in Table 1.

⋆ E-mail: jrod@msu.edu

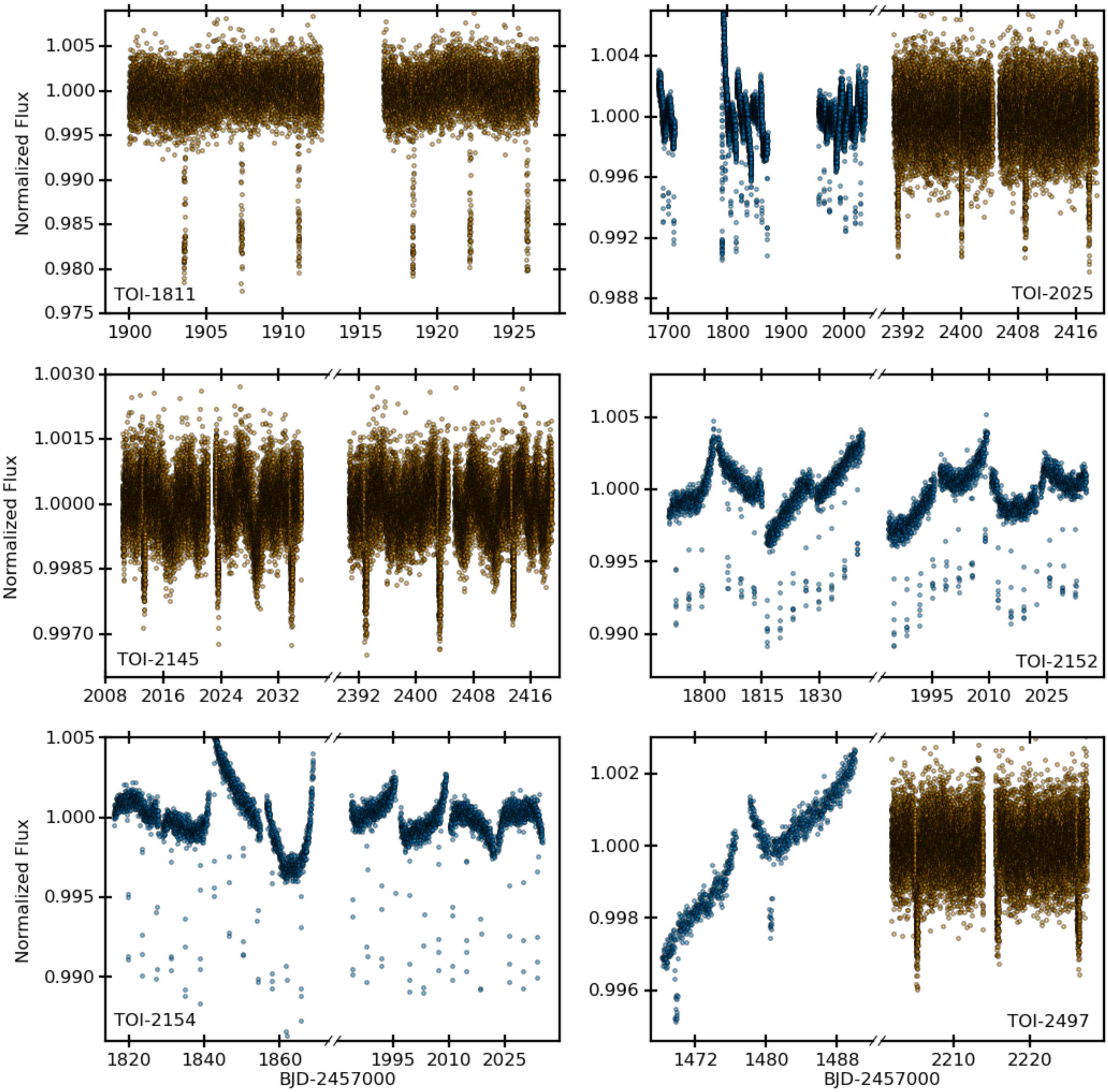

Figure 1. The *TESS* 30-minute light curves extracted using the technique described in §2.1 (blue) and 2-minute SPOC light curves (orange) for TOI-1811 (top-left), TOI-2025 (top-right), TOI-2145 (middle-left), TOI-2152 (middle-right), TOI-2154 (bottom-left), and TOI-2497 (bottom-right).

2.1 *TESS* Photometry

Launched in 2018, NASA's *TESS* mission has been in full operation with over 200 planets confirmed to date[1]. Using a 24°x96° field of view, *TESS* monitors each observing sector for ∼27 days before moving to the next sector (Ricker et al. 2015). During the prime mission, *TESS* observed nearly the entire sky at a 30-minute cadence and a pre-selected set of a few hundred thousand stars at 2-minute cadence. After a successful 2-year primary mission that observed each ecliptic hemisphere for about a year, *TESS* began its 27-month first extended mission that is ongoing and has already revisited some of the prime-mission targets but also observed a large portion of the ecliptic plane, where the repurposed *Kepler* mission (*K2*, Howell et al. 2014) discovered over 500 planetary systems and over 1000 more candidates (Barros et al. 2016; Crossfield et al. 2016; Vanderburg et al. 2016; Mayo et al. 2018; Zink et al. 2019; Hardegree-Ullman et al. 2020; Zink et al. 2021, e.g.). During the 27-month extended mission, *TESS* has added a third, 20-second cadence mode for some pre-selected targets and the exposure time of the Full Frame Images (FFI, where the entire 24°x96° field of view is observed) was reduced to 10 min-

[1] https://exoplanetarchive.ipac.caltech.edu/

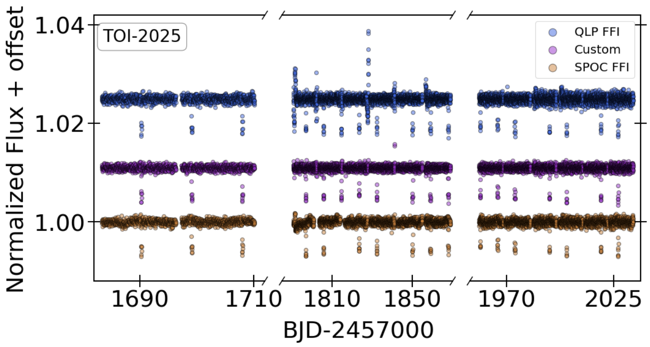

Figure 2. The flattened *TESS* 30-minute light curves reduced using with the Quick Look Pipeline (Blue, Huang et al. 2020), Custom (purple, Vanderburg et al. 2019), and flattened *TESS*-SPOC light curves generated from the FFIs (Orange, Jenkins et al. 2016; Caldwell et al. 2020) for TOI-2025.

utes. To date, *TESS* has announced over 5000 targets that display a signal consistent with it being an exoplanet, which are known as *TESS* Objects of Interest[2] (TOIs, Guerrero et al. 2021), targets that display a signal consistent with it being an exoplanet.

TESS observed all six TOIs presented here during the 2-year primary mission, and, in the cases of TOI-2025 and TOI-2497, reobserved during the extended mission. TOI-1811 and TOI-2145 were only observed at 2-minute cadence, TOI-2152 and TOI-2154 were only observed in the 30-min full frame images, and TOI-2025 and TOI-2497 were observed in both cadences during different sectors (see Figure 1). For the 2-minute observations, the *TESS* images were downlinked, reduced, and analyzed by the Science Processing Operations Center (SPOC) pipeline (Smith et al. 2012; Stumpe et al. 2014; Jenkins et al. 2016). The final SPOC lightcurves were searched for transits with the SPOC Transiting Planet Search (TPS, Jenkins 2002). The final processed lightcurves were downloaded from the Mikulski Archive for Space Telescopes (MAST) archive and included in our global fitting (see §3).

For our final transit fits, we adopt the SPOC 2-minute lightcurves when available but we re-extracted the 30-minute FFI light curves using a custom full frame image pipeline derived from that of Vanderburg et al. (2019). We downloaded the pixels surrounding the locations of each host star using the TESSCut interface (Brasseur et al. 2019) to the MAST. We first extracted light curves from a series of 20 different photometric apertures. We then removed systematic errors from each light curve by decorrelating with the mean and standard deviations of the spacecraft quaternion time series within each exposure and the *TESS* SPOC pipeline's Presearch Data Condition (PDC) cotrending basis vectors (binned to the cadence of each sector's observations). We performed the decorrelation via linear regression, where we solved for the best-fit coefficients for each model component using a matrix inversion technique, while iteratively excluding outlier points. We also included a basis spline in our linear regression model to simultaneously account for the stars' photometric variability. After subtracting the best-fit systematics components from our linear regression from the light curve, we then applied a correction for dilution from nearby stars customized for each of the 20 apertures based on a model of the *TESS* pixel response function and the known positions and magnitudes from the *TESS* Input Catalog (TIC, Stassun et al. 2018) of nearby stars. Finally, for each star we selected one of the 20 photometric apertures by finding which one minimized its photometric scatter (outside of transit) and chose that as the final light curve for each star. We compared our final FFI lightcurve of TOI-2025 with that created by the SPOC pipeline and the MIT Quick Look Pipeline (QLP, Huang et al. 2020) as a check for the lightcurve quality (see Figure 2). We adopt our custom FFI lightcurve for the final global fitting but note no significant difference in the transit properties when comparing the three versions of the FFI lightcurves. Additionally, we have photometric follow-up transits from the ground for each system other than TOI-2497.

To properly fit our *TESS* photometry within the global fit, we flatten the out-of-transit features using *Keplerspline*[3], which fits a spline to the variability seen and divides out the best-fit model (Vanderburg & Johnson 2014). The spline requires spacing for the break points (breaks in the spline to handle discontinuities) and we optimized this by following the methodology from Shallue & Vanderburg (2018) to minimize the Bayesian information criterion. Most of the out-of-transit information provides little to no useful information in determining the full system parameters in the case of these six TOIs but is still computationally intensive to model. Therefore, we remove all baseline photometry from the *TESS* lightcurves, only keeping one full transit duration before the transit until one full transit duration after each transit. In the global model, we modeled all flattened lightcurve segments for each system of a given cadence with the same zero point and added variance (see §3).

2.2 KELT Photometry

Since *TESS* focuses on observing bright (V<12) stars, there is a wealth of archival data on these targets from even small-aperture surveys like the Kilodegree Extremely Little Telescope (KELT) survey[4] (Pepper et al. 2007, 2012, 2018). See Siverd et al. (2012) & Kuhn et al. (2016) for a discussion on the KELT-North and KELT-South observing strategy and reduction techniques. KELT uses two small aperture telescopes (Mamiya 645 80mm f/1.9 lens with 42mm aperture, Apogee 4k×4k CCD) to observe most of the entire sky on a 20 to 30 minute cadence. Light curves from the KELT survey are accessible through the NASA Exoplanet Archive[5].

We do not recover the transits detected by *TESS*, likely due to a combination of the poor duty cycle from the ground (for the longer period systems, Gaudi et al. 2005), the faintness of the host stars (for the shorter period systems), and some of the transits being shallow (<0.5%). However, KELT data can be useful to measure stellar rotation periods. Following the approach of Stassun et al. (1999); Oelkers et al. (2018); Rodriguez et al. (2021), we executed a search for periodic signals using the KELT data. For these stars, we post-processed the light curve data using the Trend-Filtering Algorithm (Kovács et al. 2005) to remove common systematics. We then searched for candidate rotation signals using a modified version of the Lomb-Scargle period finder algorithm (Lomb 1976; Scargle 1982). We searched for periods between a minimum period of 0.1 days and a maximum period of 100 days using the autopower feature of the `astropy` implementation of Lomb-Scargle. We masked periods between 0.5 and 0.505 days and 0.97–1.04 days to avoid the most common detector

[2] https://tess.mit.edu/toi-releases/

[3] https://github.com/avanderburg/keplerspline

[4] https://keltsurvey.org

[5] https://exoplanetarchive.ipac.caltech.edu/cgi-bin/TblSearch/nph-tblSearchInit?app=ExoTbls&config=kelttimeseries

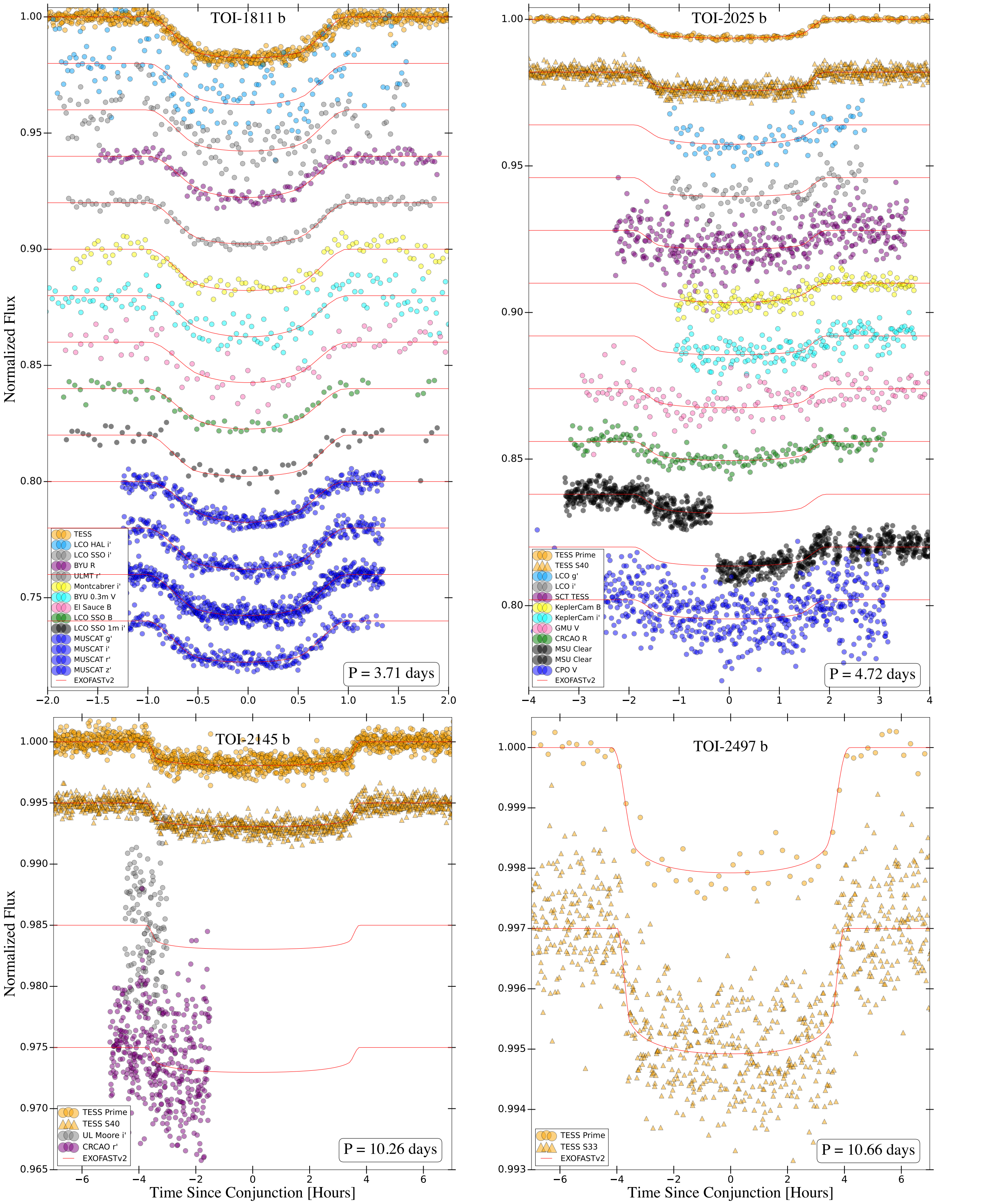

Figure 3. The *TESS* (orange) and TFOP SG1 follow-up transits of TOI-1811 b (top-left), TOI-2025 b (top-right), TOI-2145 b (bottom-left), and TOI-2497 b (bottom-right). The `EXOFASTv2` model for each transit observation is shown by the red solid line.

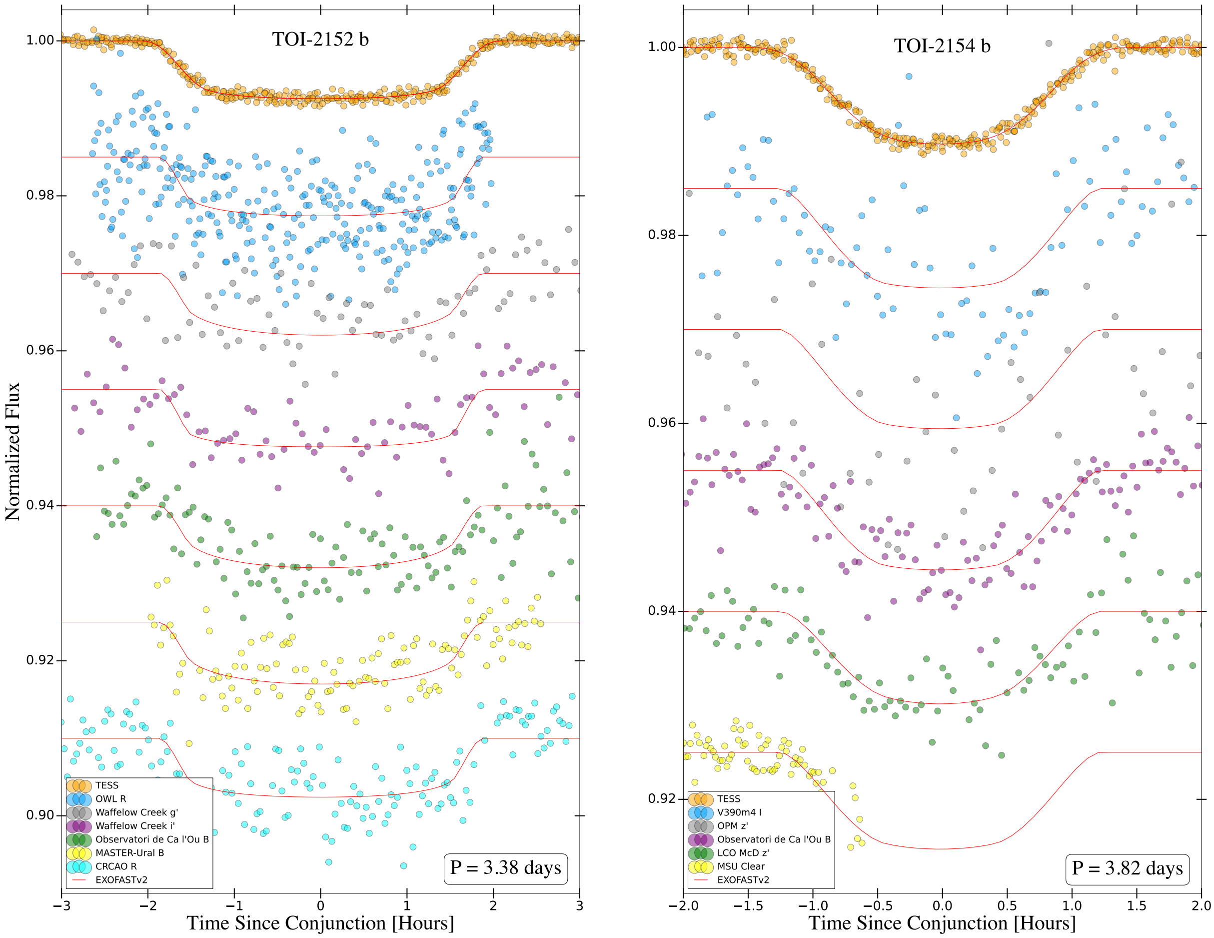

Figure 4. The *TESS* (orange) and TFOP SG1 follow-up transits of TOI-2152A b (Left) and TOI-2154 b (Right). The `EXOFASTv2` model for each transit observation is shown by the red solid line.

aliases associated with KELT's observational cadence and its interaction with the periods for the solar and sidereal day. For each star, we selected the highest statistically significant peak of the power spectrum as the candidate period for stellar variability.

We then executed a boot-strap analysis, using 100 Monte-Carlo iterations, where the dates of the observations were not changed but the magnitude values of the light curve were randomized, following the work of Henderson & Stassun (2012); VanderPlas (2018). We recalculated the Lomb-Scargle power spectrum for each iteration, and recorded the maximum peak power of all iterations. If the highest power spectrum peak was larger than the maximum simulated peak after 100 iterations, we considered the periodic signal to be a candidate rotation period. We find only TOI-1811 to have a significant candidate rotation period at 25.779 days using KELT data.

2.3 WASP Photometry

Additional observations were available for only TOI-1811 from the Wide Angle Survey for Planets (WASP) survey. Each WASP site (La Palma and SAAO) used an array of eight 200-mm, f/1.8 lenses to create a large field of view (Pollacco et al. 2006). The typical cadence of the observations were 15-30 minutes. Observations of TOI-1811 from 2007 and 2011 were available and following the techniques from Maxted et al. (2011), we searched for periodic modulation consistent with the rotation period of the star. We find a similar period to that what was in the KELT data, 23$\pm$1 days. Additionally, using the WASP search algorithm described in Collier Cameron et al. (2007) on the observations and the identification of planetary period of TOI-1811 b from *TESS*, we measure the WASP ephemeris of planet to be a period of 3.7130803$\pm$0.0000292 and a mid-transit epoch (T_C) of 2454006.04900$\pm$0.00337 HJD_{TDB}. This ephemeris is used as a prior for the `EXOFASTv2` global analysis of TOI-1811 b (see §3).

2.4 Ground-based Photometry from the *TESS* Follow-up Observing Program Working Group

As part of the confirmation processes within TFOP, we observed five of the six giant planet systems presented in this paper using a variety of small-aperture (<2 meter) telescopes to confirm the transit was on target and to refine the system parameters (particularly increasing the photometric baseline to improve our precision and accuracy on future times of transit). Observations were obtained using the Las Cumbres Observatory (LCO) telescope network (Brown et al. 2013), KeplerCam on the 1.2m telescope at Fred Lawrence Whipple Observatory (FLWO), C. R. Chambliss Astronomical Observatory (CRCAO) at Kutztown University, Brigham Young University's campus telescopes, El Sauce Observatory, MUSCAT2 on the 1.5m Telescopio Carlos Sánchez (TCS) , the University of Louisville's Moore Observatory, Michigan State University's Observatory, George Mason University's Observatory, Optical Wide-field patroL network

(OWL-Net) Oukaimeden observatory (OWL), Waffelow Creek Observatory, Observatori de Ca l'Ou, MASTER-Ural observatory, Villa '39 Observatory, Observatoire Privé du Mont (OPM), Conti Private Observatory (CPO), and Kotizarovci Observatory. Table 2 shows the information on each observatory and the detrending parameters used within the global fit. The photometric observations were reduced and aperture photometry extraction was conducted using `AstroImageJ` (Collins et al. 2017) for all follow-up transit observations except MUSCAT2 and the MASTER-Ural observations. Below we briefly review the reduction process used for these facilities. Unfortunately, due to its longer orbital period, we were not able to get photometric follow-up on TOI-2497.

Two of our follow up transit observations did not use `AstroImageJ` to perform the reduction and photometry. TOI-1811 was observed on the night of UT 2021 June 05 with the multicolor imager MuSCAT2 (Narita et al. 2019) mounted on the 1.5 m Telescopio Carlos Sánchez (TCS) at Teide Observatory, Spain. The raw data were reduced by the MuSCAT2 pipeline (Parviainen et al. 2019) which performed a standard image calibration and aperture photometry. TOI-2152 was observed on UT 2020 December 12 with MASTER-Ural 0.4m telescope. The data reduction included standard dark, flat field and astrometry corrections, and is performed using the MASTER-Ural pipeline[6]. Comparison stars were selected from the *Gaia* DR2 catalog. Aperture photometry of the object and the ensemble of comparison stars was performed using Python/Photutils (Bradley et al. 2019). Photometric data processing and detrending was completed with the Python version of the Astrokit (Burdanov et al. 2014), to minimize the standard deviation of the ensemble of comparison stars.

2.5 Spectroscopy

To confirm these six systems as bona fide transiting giant planets by removing any remaining false positive scenario, we obtained time-series spectroscopic measurements of each target coordinated through TFOP. These radial velocity measurements, combined with the transit photometry, allowed us to precisely measure the mass and orbital eccentricity of each system, a key component in understanding their evolutionary origins. Table 3 shows a sample radial velocity (RV) point per target per instrument (the full table will be available in machine-readable form in the online journal). The RVs and best-fit models from our `EXOFASTv2` analysis are shown in Figure 5 (see §3).

2.5.1 TRES Spectroscopy

Using the Tillinghast Reflector Echelle Spectrograph (TRES; Fűrész 2008)[7] on the 1.5m Tillinghast Reflector, we measured the radial velocity orbit of all six TOIs presented in this paper. The telescope and spectrograph are located at the Fred L. Whipple Observatory (FLWO) on Mt. Hopkins, AZ. The reduction and RV analysis followed the procedure described in Buchhave et al. (2010) and Quinn et al. (2012), with the bisector analysis following the work of Torres et al. (2007). The only difference is that the template spectra for the RV extraction were created by median-combining all of the out-of-transit spectra (after shifting each to align them). The TRES spectra were also analyzed using the Stellar Parameter Classification (SPC) package (Buchhave et al. 2012) to determine the [Fe/H], $T_{\rm eff}$, and rotational velocity of each host star (see Tables 1 and 6).

[6] `https://master.kourovka.ru/`
[7] `http://www.sao.arizona.edu/html/FLWO/60/TRES/GABORthesis.pdf`

2.5.2 CHIRON Spectroscopy

We also observed TOI-2497 on 9 separate nights using the 1.5 m SMARTS / CHIRON facility to measure the mass and orbital eccentricity of the companions, and constrain the host star parameters (Tokovinin et al. 2013; Paredes et al. 2021). CHIRON is located at Cerro Tololo Inter-American Observatory (CTIO) Chile, and is a high resolution échelle spectrograph fed with an image slicer through a single multi-mode fiber corresponding to a spectral resolving power of $R \sim 80{,}000$ (4100 to 8700Å). The RVs were derived using a least-squares deconvolution (Donati et al. 1997; Gray 2005; Zhou et al. 2020) of the observed spectra against a non-rotating synthetic templates. These templates were generated using the ATLAS9 model atmospheres (Kurucz 1992) and matched the spectral parameters of each host star.

2.5.3 MINERVA Australis Spectroscopy

We make use of the Minerva-Australis array for additional radial velocities of TOI-2497. Minerva-Australis is an array of four identical 0.7 m telescopes located at Mt Kent Observatory, Australia. The telescopes are fed by four independent fibers into the KiwiSpec high resolution échelle spectrograph, yielding a spectral resolving power of R$\sim$80,000 over the wavelength range of 5000-6300Å (Addison et al. 2019). Simultaneous wavelength calibration is provided by two calibration fibers, illuminated by a quartz lamp through an iodine cell, that tracks the instrument drift over an exposure. Radial velocities are measured from each telescope independently via a least-squares deconvolution between the extracted spectra and a synthetic, following the procedure described in Zhou et al. (2021). The template is generated from an ATLAS9 atmosphere model (Castelli & Hubrig 2004) at the atmosphere parameters of the target star, and has no rotational broadening applied. The resulting line-broadening function is modeled with a kernel describing the rotational, macroturbulent, and instrumental broadening effects, as well as the radial velocity shift of a given exposure.

2.5.4 MINERVA North Spectroscopy

The MINERVA North observations of TOI-2145 were made with the MINERVA telescope array and KiwiSpec Spectrograph (Wilson et al. 2019; Swift et al. 2015), which consists of four robotic telescopes at Whipple Observatory in Arizona, fiber fed to a temperature and pressure stabilized, R$\sim$80,000, iodine cell calibrated spectrograph. We obtained 24 observations with T1, 16 observations with T2, and 5 observations with T3 spanning from UT 2020 May 09 to UT 2021 May 31. We extracted 1D spectra from the 2D spectra with our standard methods.

The corresponding MINERVA RVs are computed from the 1D spectra with `pychell` using updated methods compared to those described in Cale et al. (2019). Each 1-dimensional spectrum is forward modeled on a per-order basis. The model accounts for the wavelength solution, instrumental profile (IP), continuum, tellurics, and stellar Doppler shift. An iodine vapor gas cell in the calibration unit constrains the wavelength solution and IP. We use the Fourier Transform Spectrometer (FTS) scan measured at NIST, described in Wilson et al. (2019). A synthetic BT-Settl model ($T_{\rm eff}$ = 6000 K, $\log g = 3.5$, $(Fe/H)_\odot = 0$) is used as an initial stellar template, which is further Doppler broadened to $v \sin i = 19$ km s^{-1} with PyAstronomy (Czesla et al. 2019). `pychell` then iteratively updates this template based on the residuals between the data and model, and although the fits suggest the stellar template is more accurate at

Table 1. Literature and Measured Properties

Other identifiers								
		TOI-1811	TOI-2025	TOI-2145	TOI-2152	TOI-2154	TOI-2497	
		TIC 376524552	TIC 394050135	TIC 88992642	TIC 395393265	TIC 428787891	TIC 97568467	
		—	—	HIP 86040	—	—	—	—
	TYCHO-2	TYC 1992-00307-1	TYC 4595-00797-1	TYC 3091-00842-1	TYC 4498-01400-1	TYC 4617-00138-1	TYC 0725-01745-1	
	2MASS	J12354142+2712518	J18511077+8214436	J17350195+4041421	J01452120+7747244	J04440676+8421511	J06001500+1153030	
	TESS Sector	[22]	[14, 18, 19, 20, 24, 25, 26, 40]	[25, 26, 40]	[18, 19, 25, 26]	[19, 20, 25, 26]	[6, 33]	
Parameter	**Description**	**Value**	**Value**	**Value**	**Value**	**Value**	**Reference**	
α_{J2000}‡	Right Ascension (RA)	12:35:41.419	18:51:10.840	17:35:01.950	01:45:21.218	04:44:06.869	06:00:15.008	1
δ_{J2000}‡	Declination (Dec)	+27:12:51.923	+82:14:43.562	+40:41:42.205	+77:47:24.623	+84:21:51.119	+11:53:03.031	1
G	Gaia G mag.	11.76±0.02	11.36±0.02	8.94±0.02	11.24±0.02	11.04±0.02	9.47±0.02	1
B_P	Gaia B_P mag.	12.33±0.02	11.69±0.02	9.24±0.02	11.68±0.02	11.32±0.02	9.73±0.02	1
R_P	Gaia R_P mag.	11.07±0.02	10.90±0.03	8.52±0.02	10.65±0.02	10.61±0.02	9.10±0.02	1
T	TESS mag.	11.1237±0.0061	10.9461±0.0061	8.5594±0.0063	10.7053±0.0061	10.6611±0.0085	9.1411±0.0063	2
J	2MASS J mag.	10.280±0.024	10.380±0.025	8.021±0.020	9.973±0.026	10.154±0.025	8.697±0.021	3
H	2MASS H mag.	9.732±0.027	10.071±0.028	7.810±0.023	9.669±0.30	9.864±0.027	8.533±0.020	3
K_S	2MASS K_S mag.	9.643±0.025	10.010±0.021	7.761±0.031	9.597±0.024	9.850±0.025	8.486±0.020	3
WISE1	*WISE1* mag.	9.579±0.030	9.995±0.030	7.706±0.030	9.535±0.030	9.808±0.030	8.418±0.030	4
WISE2	*WISE2* mag.	9.668±0.030	10.037±0.030	7.745±0.030	9.543±0.030	9.836±0.030	8.448±0.030	4
WISE3	*WISE3* mag.	9.590±0.042	9.973±0.042	7.717±0.030	9.470±0.032	9.771±0.038	8.424±0.030	4
WISE4	*WISE4* mag.	—	—	7.691±0.122	8.968±0.304	—	8.47±0.365	4
μ_α	Gaia DR2 proper motion in RA (mas yr^{-1})	-45.874±0.058	2.791±0.036	-6.512±0.035	27.643±0.040	-10.783±0.036	12.502±0.076	1
μ_δ	Gaia DR2 proper motion in DEC (mas yr^{-1})	-10.766±0.035	-4.521±0.045	-3.281±0.040	-11.634±0.048	15.218±0.043	-27.310±0.064	1
$v \sin i_\star$	Rotational velocity (km s^{-1})	3.3±0.5	7.3±0.5	19.4±0.5	5.4±0.5	5.4±0.5	39.6±1.0	§2.5.1& §2.5.1
$\pi^\dagger$	Gaia DR2 Parallax (mas)	7.801±0.051	2.978±0.031	4.451±0.031	3.302±0.042	3.374±0.034	3.507±0.051	1

NOTES: The uncertainties of the photometry have a systematic error floor applied.
‡ RA and Dec are in epoch J2000. The coordinates come from Vizier where the Gaia RA and Dec have been precessed and corrected to J2000 from epoch J2015.5.
† Values have been corrected for the -0.30 μas offset as reported by Lindegren et al. (2018) but this is not significant for these systems.
References are: [1]Gaia Collaboration et al. (2018),[2]Stassun et al. (2018),[3]Cutri et al. (2003), [4]Cutri et al. (2012)

later iterations, the corresponding RVs are inconsistent with the orbit of the planet, whereas the initial BT-Settl template yields consistent RVs with the TRES observations which strongly support the planetary orbit. We checked that the MINERVA North observations were consistent with TRES by running a global fit with only the TRES observations, and saw no discrepancy. We have yet to find cause for the loss of accuracy at later iterations, and is a subject of future work. We therefore use RVs from the first iteration. The RMS of the residuals of our adopted RV model suggest a median S/N per-spectral pixel of 17.

2.6 High Resolution Imaging

As part of our standard process for validating transiting exoplanets to assess the possible contamination of bound or unbound companions on the derived planetary radii (Ciardi et al. 2015), we observed the TOIs with a combination of high-resolution imaging resources including near-infrared adaptive optics (AO) imaging at Lick (TOI-2145, TOI-2497) and Palomar (TOI-1811, TOI-2145) Observatories and with optical speckle imaging using the 2.5m SAI telescope (TOI-1811, TOI-2025, TOI-2145, TOI-2152, TOI-2154) and the Southern Astrophysical Research (SOAR) telescope (TOI-2497). While the optical speckle observations tend to provide higher resolution, the NIR AO obsevations tend to provide better sensitivity, especially to lower-mass stars. If a companion is detected, the combination of the observations in multiple filters enables better characterization. Additionally, recent studies have shown that Gaia (DR2 and eDR3) (Gaia Collaboration et al. 2018) is most efficient at identifying companions with separations greater than $\sim 0.5 - 1''$ (Ziegler et al. 2018). Gaia eDR3 (Gaia Collaboration et al. 2021) is also used to identify targets that have a large Renormalised Unit Weight Error (RUWE) value indicative of a poor astrometric fit assuming a single-star model and possibly indicating the presence of undetected stellar companions. For all of the observations, We only detect one faint companion to TOI-2152 (ΔMag ~ 5) within $1''$ of the primary target.

2.6.1 *Summary of AO Observations*

The Palomar Observatory observations of TOI-1811 and TOI-2145 were made with the PHARO instrument (Hayward et al. 2001) behind the natural guide star AO system P3K (Dekany et al. 2013) on UT 2021 February 23 and UT 2021 February 24, respectively, in a standard 5-point quincunx dither pattern with steps of $5''$ in the narrow-band $Br-\gamma$ filter ($\lambda_o = 2.1686; \Delta\lambda = 0.0326$ μm). Each dither position was observed three times, offset in position from each other by $0.5''$ for a total of 15 frames; with an integration time of 30 and 1.4 seconds per frame, respectively for total on-source times of 450 and 21 seconds. PHARO has a pixel scale of $0.025''$ per pixel for a total field of view of $\sim 25''$.

We also observed TIC 88992642 (TOI-2145) and TIC 97568467 (TOI-2497) on UT 2021 March 29 using the ShARCS camera on the Shane 3-meter telescope at Lick Observatory (Kupke et al. 2012; Gavel et al. 2014; McGurk et al. 2014). Observations were taken with the Shane adaptive optics system in natural guide star mode

Table 2. Photometric follow-up observations of these systems used in the global fits and the detrending parameters.

Target	Observatory	Date (UT)	size (m)	Filter	FOV	Pixel Scale	Exp (s)	Additive Detrending
TOI-1811 b	LCO SSO	2020 April 23	0.4	i'	$19' \times 29'$	$0.57''$	55	airmass
TOI-1811 b	LCO HAL	2020 April 23	0.4	i'	$19' \times 29'$	$0.57''$	55	airmass
TOI-1811 b	BYU	2020 April 27	0.6	R	$32' \times 32'$	$0.93''$	70	airmass
TOI-1811 b	ULMT	2020 April 27	0.6	i'	$26.8' \times 26.8'$	$0.395''$	128	airmass
TOI-1811 b	Montcabrer	2020 April 27	0.3	i'	$45.8' \times 45.8'$	$0.9''$	120	airmass
TOI-1811 b	BYU-12	2020 May 08	0.6	V	$25' \times 19'$	$0.92''$	90	airmass
TOI-1811 b	El Sauce	2020 May 12	0.36	B	$19' \times 13'$	$1.47''$	180	airmass
TOI-1811 b	LCO SSO	2021 February 25	1.0	z'	$27' \times 27'$	$0.39''$	55	airmass
TOI-1811 b	LCO SSO	2021 February 25	1.0	B	$27' \times 27'$	$0.39''$	70	airmass
TOI-1811 b	MUSCAT2	2021 June 05	1.52	g'	$7.4' \times 7.4'$	$0.44''$	30	airmass
TOI-1811 b	MUSCAT2	2021 June 05	1.52	i'	$7.4' \times 7.4'$	$0.44''$	30	airmass
TOI-1811 b	MUSCAT2	2021 June 05	1.52	r'	$7.4' \times 7.4'$	$0.44''$	15	airmass
TOI-1811 b	MUSCAT2	2021 June 05	1.52	z'	$7.4' \times 7.4'$	$0.44''$	30	airmass
TOI-2025 b	Kotizarovci	2020 June 26	0.3	*TESS*	$15' \times 23'$	$1.2064''$	30	airmass
TOI-2025 b	LCO TFN	2020 June 26	0.4	i'	$19' \times 29'$	$0.57''$	60	airmass
TOI-2025 b	LCO TFN	2020 June 26	0.4	g'	$19' \times 29'$	$0.57''$	60	airmass
TOI-2025 b	FLWO/KeplerCam	2021 May 12	1.2	B	$23.1' \times 23.1'$	$0.672''$	20	airmass
TOI-2025 b	FLWO/KeplerCam	2021 May 12	1.2	i'	$23.1' \times 23.1'$	$0.672''$	7	airmass
TOI-2025 b	GMU	2021 May 21	0.8	R	$23' \times 23'$	$0.34''$	50	airmass
TOI-2025 b	CRCAO	2021 May 21	0.61	R	$19.5' \times 13'$	$0.39''$	120	airmass
TOI-2025 b	MSU	2021 September 30	0.61	*Clear*	$26.8' \times 26.8'$	$0.55''$	20	None
TOI-2025 b	MSU	2021 October 18	0.61	*Clear*	$26.8' \times 26.8'$	$0.55''$	30	None
TOI-2025 b	CPO	2021 December 29	0.61	V	$23' \times 18'$	$1''$	30	total counts
TOI-2145 b	CRCAO	2021 Sept 07	0.61	r'	$19.5' \times 13'$	$0.39''$	20	airmass
TOI-2145 b	Moore	2021 Sept 07	0.61	i'	$26.8' \times 26.8'$	$0.39''$	20	airmass
TOI-2152 b	OWL	2020 August 17	0.5	B	$1.1^\circ \times 1.1^\circ$	$1'$	20	airmass
TOI-2152 b	Waffelow Creek	2020 October 11	0.36	g'	$27' \times 15'$	$0.66''$	90	airmass
TOI-2152 b	Waffelow Creek	2020 October 11	0.36	i'	$27' \times 15'$	$0.66''$	90	airmass
TOI-2152 b	Observatori de Ca l'Ou	2020 November 24	0.4	B	$19' \times 19'$	$1.14''$	150	airmass
TOI-2152 b	MASTER-Ural	2020 December 12	0.4	R	$2^\circ \times 2^\circ$	$1.85''$	80	airmass
TOI-2152 b	CRCAO	2021 June 28	0.61	R	$19.5' \times 13'$	$0.39''$	120	airmass
TOI-2154 b	V39-0m4	2020 August 18	0.4	I	$32' \times 32'$	$0.95''$	60	airmass
TOI-2154 b	OPM	2020 October 29	0.2	z'	$39' \times 29'$	$0.69''$	180	airmass
TOI-2154 b	Observatori de Ca l'Ou	2020 November 23	0.4	B	$19' \times 19'$	$1.14''$	110	airmass
TOI-2154 b	LCO McDonald	2020 December 03	1.0	z'	$27' \times 27'$	$0.39''$	45	airmass
TOI-2154 b	MSU	2021 October 24	0.61	*Clear*	$26.8' \times 26.8'$	$0.55''$	60	airmass
TOI-2497 b	None							

NOTES: All the follow-up photometry presented in this paper is available in machine-readable form in the online journal. See §D in the appendix of Collins et al. (2017) for a description of each detrending parameter.

in order to search for nearby, unresolved stellar companions. For each target, we collected sequences of observations using a *Ks* filter ($\lambda_0 = 2.150$ μm, $\Delta\lambda = 0.320$ μm) and a J filter ($\lambda_0 = 1.238$ μm, $\Delta\lambda = 0.271$ μm). We reduced the data using the publicly available `SImMER` pipeline (Savel et al. 2020).[8] We find no nearby stellar companions within our detection limits.

The AO data were processed and analyzed with a custom set of IDL tools. The science frames were flat-fielded and sky-subtracted. The flat fields were generated from a median average of dark subtracted flats taken on-sky. The flats were normalized such that the median value of the flats is unity. The sky frames were generated from the median average of the 15 dithered science frames; each science image was then sky-subtracted and flat-fielded. The reduced science frames were combined into a single combined image using an intra-pixel interpolation that conserves flux, shifts the individual dithered frames by the appropriate fractional pixels, and median-coadds the frames. The final resolutions of the combined dithers were determined from the FWHM of the point spread functions for each of the stars: $0.102''$ for TOI-1811 and $0.092''$ for TOI-2145. The sensitivities of the final combined AO image were determined by injecting simulated sources azimuthally around the primary target every 20° at separations of integer multiples of the central source's FWHM (Furlan et al. 2017). The brightness of each injected source was scaled until standard aperture photometry detected it with 5σ significance. The resulting brightness of the injected sources relative to primary target set the contrast limits at that injection location. The final 5σ limit at each separation was determined from the average of limits at that separation (across all azimuthal samples) and the uncertainty on the limit was set by the rms dispersion of the azimuthal slices at a given radial distance. For both TOI-1811 and TO-2145, no additional stellar companions were detected in agreement with the other observations.

[8] https://github.com/arjunsavel/SImMER

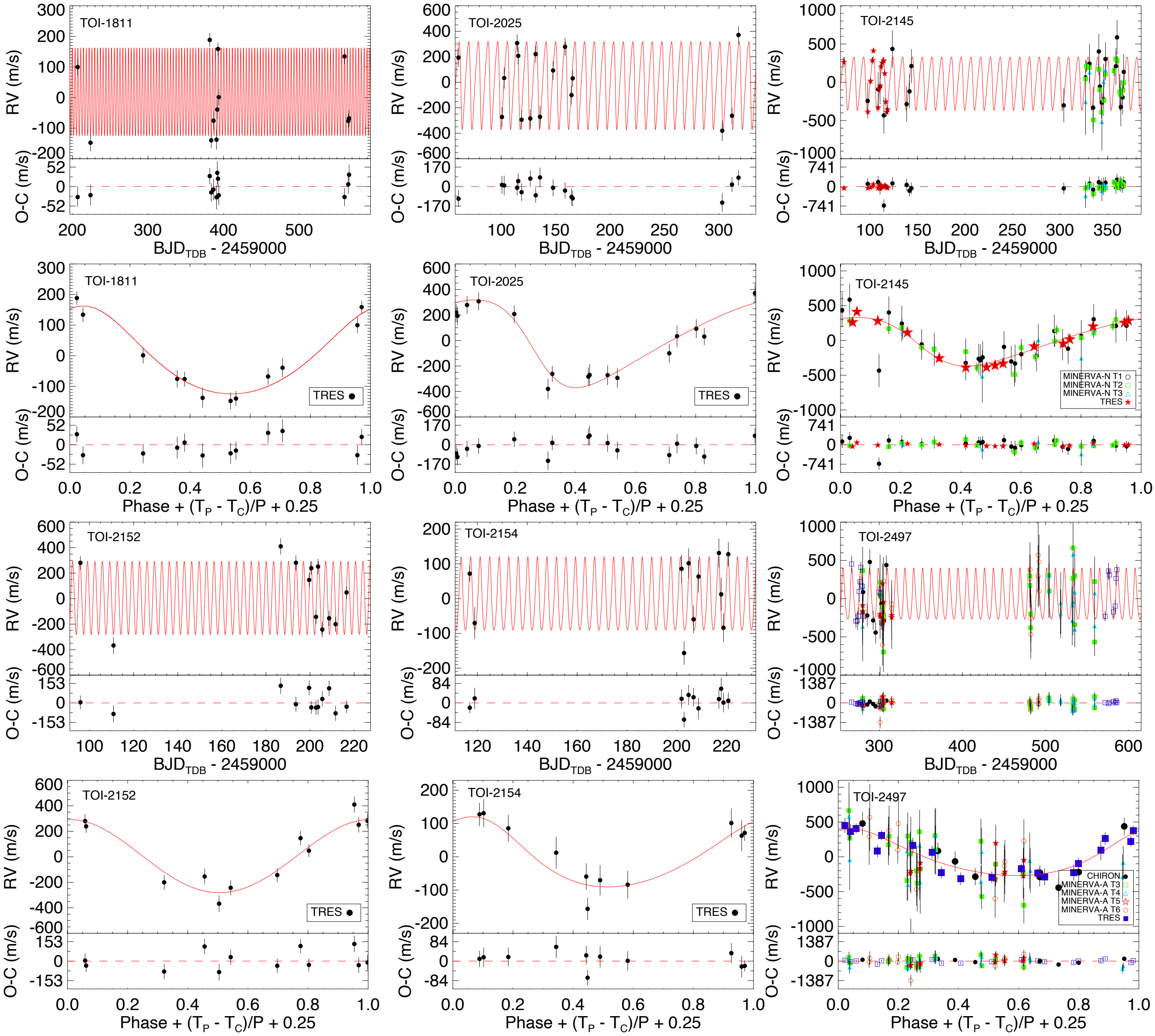

Figure 5. The RV observations of TOI-1811 (top-left), TOI-2025 (top-middle), TOI-2145 (top-right), TOI-2152 (bottom-left), TOI-2154 (bottom-middle), and TOI-2497 (bottom-right). In each case, the top figure shows the RVs vs time and the bottom panel is phased to the best-fit ephemeris from our global fit. The EXOFASTv2 model is shown in red and the residuals to the best-fit are shown below each plot.

2.6.2 *Speckle Imaging*

Using the 4.1-m SOAR telescope, we obtained speckle imaging of TOI-2497 using HR Cam on UT 2021 February 27 in the I-band following the observing and reduction strategy described in Tokovinin (2018). HRCam on SOAR has a $15'' \times 15''$ field of view and had a $0.01575''$ pixel scale. With a contrast of ΔMag of 7.7 at $1''$, we detected no nearby companions around TOI-2497. For a complete description of the observing strategy for *TESS* targets, see Ziegler et al. (2020).

TOI-1811, TOI-2025, TOI-2145, TOI-2152, and TOI-2154 were observed with the Speckle Polarimeter (Safonov et al. 2017) on the 2.5 m telescope at the Caucasian Observatory of Sternberg Astronomical Institute (SAI) of Lomonosov Moscow State University. SPP uses Electron Multiplying CCD Andor iXon 897 as a detector. The atmospheric dispersion compensator allowed observation of relatively faint targets through the wide-band I_c filter. For TOI-2145 we used a medium band interference filter with FWHM of 50 nm and centered on 625 nm. The power spectrum was estimated from 4000 frames with 30 ms exposure. The detector has a pixel scale of 20.6 mas pixel^{-1}. For all targets except for TOI-2152 we did not detect stellar companions, the contrast limits at $1''$ are Δmag = 6.7 (TOI-1811), 6.4 (TOI-2025), 3.3 (TOI-2145), 5.9 (TOI-2152, this had multiple observations ranging from 4.7 to 6.3), and 6.5 (TOI-2154). We note that the difference image analysis performed in the data validation reports from *TESS* show that the source of the transit signal for TOI-2145 was located within $5.0 \pm 2.7''$ and for TOI-1811 was within $1.78 \pm 2.5''$, complementing the high resolution imaging results.

TOI-2152 is the only star that we found to have a close-in stellar companion. The separation, position, and contrast of the TOI-2152 inner companion were estimated on 4 dates; the results are presented in Table 4. According to proper motion from Gaia eDR3, the pri-

Table 3. One RV point from each spectrograph for all six systems. The full table of RVs for each system is available in machine-readable form in the online journal.

BJD_{TDB}	RV (m s^{-1})	$\sigma^{\dagger}_{RV}$ (m s^{-1})	Target	Instrument
2459206.966936	-91.2	24.7	TOI-1811	TRES
2459060.767111	395.0	39.8	TOI-2025	TRES
2459097.65584	-194.7	103.1	TOI-2145	MINERVA T1
2459326.76336	311.8	51.8	TOI-2145	MINERVA T2
2459330.93081	94.6	167.0	TOI-2145	MINERVA T3
2459072.693111	70.6	60.6	TOI-2145	TRES
2459095.870551	481.26	40.01	TOI-2152	TRES
2459201.888606	90.4	43.7	TOI-2154	TRES
2459279.908926	56275.1	271.6	TOI-2497	M-Australis T3
2459504.223682	56250.9	316.1	TOI-2497	M-Australis T4
2459279.908926	56019.7	340.9	TOI-2497	M-Australis T6
2459271.812986	-634.1	71.0	TOI-2497	TRES

NOTES:[†] The internal RV error for the observation shown.

mary star is expected to move by 22 ± 0.02 mas over the period of our observations, from UT 2020 October 21 to UT 2021 July 17; however, there apparent motion is only 13 ± 11 mas which is consistent with no discernible separation change. While not definitive, the companion appears to be a common proper motion companion and is likely gravitationally bound. With a contrast of $\Delta I = 4.8$ mag, the detection is consistent with the companion being an M1V star (($M \sim 0.5 M_{\odot}$; $T_{eff} \sim 3600K$; Pecaut & Mamajek 2013b). At a distance of $\sim$ 320pc, the companion has a projected separation of $\sim$ 250au. Interestingly, TOI-2152 also has another companion further out detected by Gaia with an angular separation of $\sim 20''$ ($\sim$ 6000au; see §2.7).

2.7 Gaia Assessment

In addition to the high resolution imaging, we have utilized Gaia to identify any wide stellar companions that may be bound members of the system. Typically, these stars are already in the *TESS* Input Catalog and their flux dilution to the transit has already been accounted for in the transit fits and associated derived parameters. Based upon similar parallaxes and proper motions (Mugrauer & Michel 2020, 2021), the only TOI in our sample which appears to have a wide stellar companion is TOI-2152 (in addition to the close-in companion identified in §2.6.2); the wide companion TIC 395393263 (Gaia DR3 562112709676597376) is $20''$ to the NW ($PA \approx 300^{\circ}$) which corresponds to a projected physical separation of $\sim 6000au$. The companion has a mass and temperature consistent with an M4V star ($M \sim 0.24 M_{\odot}$; $T_{eff} \sim 3223K$ Mugrauer & Michel 2021) – for such a small star at such a large separation, the stellar companion does not affect the stability of the planets or the measured radial velocities. Interestingly, the projected positions on the sky of the three stars are not in a line indicating that the mutual inclination of the two stellar companions is non-zero - astrometric and/or radial velocity observations would be needed to determine if the transiting planet is aligned or not with either of the two stellar companions. A summary of the hierarchical triple TOI-2152 is given in Table 5.

Gaia DR3 astrometry (Gaia Collaboration et al. 2021) provides additional information on the possibility of inner companions that may have gone undetected by either Gaia DR2 data or the high resolution imaging. The Gaia Renormalised Unit Weight Error (RUWE) is a metric, similar to a reduced chi-square, where values that are $\lesssim 1.4$ indicate that the Gaia astrometric solution is consistent with the star being single whereas RUWE values $\gtrsim 1.4$ may indicate an astrometric excess noise, possibly caused the presence of an unseen

Table 4. Binarity parameters of TOI-2152B on the basis of SPP observations: separation, position angle and magnitude difference in I band.

Date (UT)	ρ''	P.A.°	Δm
2020 Oct 21	0.765 ± 0.008	85.2 ± 0.2	4.8 ± 0.2
2020 Oct 28	0.762 ± 0.009	86.1 ± 0.3	4.8 ± 0.1
2020 Dec 02	0.770 ± 0.008	87.0 ± 0.2	4.8 ± 0.1
2021 Jul 17	0.782 ± 0.008	85.8 ± 0.2	4.6 ± 0.1

NOTES: The $\rho,''$ is the projected separation of the neighbor, if at the distance of the primary star.

companion (e.g., Ziegler et al. 2020). All of the TOIs in this sample, except TOI 1811, have RUWE values of < 1.1 indicating that the astrometric fits are consistent with the single star model. The RUWE for TOI-1811 is 1.66; there is no clear fixed boundary for when the RUWE unambiguously identifies the presence of an unseen stellar companion. The transit of TOI-1811 is very deep (19 mmag in the *TESS* light curves) and with a short orbital period of 3.7 days, it may be the transit of the planet itself that is affecting the Gaia RUWE value.

3 EXOFASTv2 GLOBAL FITS

Following the same strategy laid out in §3 of Rodriguez et al. (2021), we globally fit the RVs, *TESS* and TFOP photometry (see Figures 3, 4, & 5; and §2) for TOI-1811 b, TOI-2025 b, TOI-2145 b, TOI-2152A b, TOI-2154 b, and TOI-2497 b with `EXOFASTv2` (Eastman et al. 2013, 2019) to determine their individual system parameters and place them in context with the known exoplanet population. The Spectral Energy Distribution (SED) and the MESA Isochrones and Stellar Tracks (MIST) stellar evolution models (Paxton et al. 2011, 2013, 2015; Choi et al. 2016; Dotter 2016) were included to constrain the host star's parameters within the fit, and we account for the 30 minute smearing in the *TESS* FFI lightcurves. We enforced a systematic limit on the precision broad-band photometry (see Table 1, Stassun & Torres 2016) and use `EXOFASTv2`'s default lower limit on the systematic error on the bolometric flux (F_{bol} ∼3%). We adopted a Gaussian prior on the [Fe/H], parallax from Gaia DR2 (Gaia Collaboration et al. 2016, 2018, correcting for the offset reported by Lindegren et al. 2018), and an upper bound on the line of sight extinction from Schlegel et al. (1998) & Schlafly & Finkbeiner (2011). Both SPOC and our custom pipeline correct the *TESS* photometry for known nearby blended stars in the aperture. To allow some flexibility while checking this correction, we fit for dilution term on the *TESS* band, and placed a Gaussian prior of 0±10% of the contamination ratio reported by the *TESS* Input Catalog (TIC, Stassun et al. 2018). We saw no evidence of any significant dilution in TOI-1811, TOI-2025, TOI-2152, and TOI-2154. Unfortunately, without an independent full transit for TOI-2145 and TOI-2497, we are not able to perform this test with the limited amount of photometric follow-up. We use the recommended convergence criteria by Eastman et al. (2019) of a Gelman-Rubin statistic (<1.01) and independent draws (>1000). The results for each system are in Tables 6, 7, & 8 and in Figures 3, 4, & 5.

Table 5. Estimated Parameters for TOI-2152 Stellar Components

Stellar Component	Separation [au]	Mass $[M_\odot]$	Radius $[R_\odot]$	T_{eff} [K]	Spectral Type	Notes
TOI-2152A	···	1.52	1.61	6630	F4V	Table 6
TOI-2152B	250	0.5	0.4	3600	M1V	Pecaut & Mamajek (2013a); Boyajian et al. (2012)
TOI-2152C	6000	0.24	0.2	3200	M4V	Mugrauer & Michel (2020); Boyajian et al. (2012)

4 DISCUSSION

The combination of precision, baseline, and cadence of *TESS* will provide the ability to create a magnitude-complete, self-consistent catalog of exoplanetary systems to investigate questions about formation and evolution, and directly test tentative trends seen in the current population (Nelson et al. 2017; Rodriguez et al. 2021; Ikwut-Ukwa et al. 2022). These six new hot and warm giant planets increase the current sample of systems with precise mass and eccentricity measurements. We first review our results on each system and then discuss the impact *TESS* has made on the field of giant exoplanets. In all six systems, we see no significant inflation ($R_P > 1.5\ R_\odot$).

4.1 Review of Six New Discoveries

Orbiting an early K-star, TOI-1811 b is a hot Jupiter on a 3.71 day period that shows no signs of inflation relative to the known population ($R_P = 1.002^{+0.026}_{-0.024}\ R_J$ and $M_P = 0.974^{+0.075}_{-0.076}\ M_J$). The host star has a relatively high metallicity ([Fe/H] = $0.320^{+0.075}_{-0.077}$ dex), and the lack of a significant eccentricity is consistent with the very short tidal circularization timescale of 700±14 Myr (Adams & Laughlin 2006) and that the host star parameters suggest a main-sequence star with an age well above this.

TOI-2025 b is a super Jupiter mass ($M_P = 3.51^{+0.36}_{-0.35}\ M_J$) planet on an 8.872 day period around an early-G star. We detect a moderate, but significant eccentricity, e = $0.220^{+0.052}_{-0.053}$. Given the long circularization timescale (see Table 6) and the detected eccentricity, it is possible that TOI-2025 b migrated to its current location through dynamical interactions (e.g., Dawson & Fabrycky 2010).

Orbiting a bright (G = 8.94±0.02 mag), sub-giant ($\log g$ = $3.798^{+0.023}_{-0.026}$ cgs), TOI-2145 is a massive ($M_P = 5.35^{+0.32}_{-0.35}\ M_J$) warm Jupiter on an eccentric (e = $0.182^{+0.039}_{-0.049}$) on a 10.261 day orbit. Of the known transiting planets to date, TOI-2145 b joins only five other known planets to have a mass above 3 M_J and orbit a subgiant ($\log g$ < 4.0 cgs), but it orbits the brightest star of that group, a valuable aspect for future detailed characterization.

TOI-2152A b and TOI-2154 b are both hot Jupiters orbiting similar main-sequence F-stars at similar distances from the Sun. TOI-2152A b is a massive Jupiter ($M_P = 2.83^{+0.38}_{-0.37}\ M_J$) while TOI-2154 b is only $0.92^{+0.19}_{-0.18}\ M_J$. We see no evidence of any significant eccentricity (TOI-2152A b $e = 0.057^{+0.068}_{-0.040}$, TOI-2154 b $e = 0.117^{+0.10}_{-0.079}$) from our results but note that these two planets provide a nice comparative study since their host stars and the planets share many similar characteristics, but a significant difference in the planet's mass.

The last system in our sample is TOI-2497 b, another very massive ($M_P = 5.21 \pm 0.52\ M_J$) warm Jupiter on a 10.656 day period. Its host star, TOI-2497, is a rapidly rotating ($v \sin I_* = 39.6 \pm 1.0$ km s^{-1}) early F-star ($T_{\rm eff} = 7360^{+290}_{-270}$, that has possibly left the main sequence ($\log g = 3.963^{+0.040}_{-0.039}$ cgs). The host star is also bright (G = 9.47±0.02 mag), and combined with the rapid rotation, TOI-2497 b is an excellent target for future Doppler spectroscopy, using observations of the Rossiter McLauglin effect (Rossiter 1924; McLaughlin 1924) or Doppler tomography (e.g., Miller et al. 2010; Johnson et al. 2014; Zhou et al. 2016) to measure the projected spin-orbit alignment of the planet's orbit.

4.2 *TESS*'s impact on Giant Planets

As NASA's *TESS* mission continues to observe, it is expected to discover thousands of giant planets over its lifetime (Sullivan et al. 2015; Barclay et al. 2018), while providing great value to already known systems (Ikwut-Ukwa et al. 2020; Edwards et al. 2021; Kane et al. 2021). This is highly dependent on the number of extended missions that *TESS* is given. Even in the ∼4 years since its launch, *TESS* has discovered over 200 planets[9], of which 47 are above 0.4 M_J, nearly 10% of the known transiting giant planet population (See Figure 6). As multiple efforts, including ours, continue to confirm and characterize new transiting giant planets, it will lead to a magnitude-complete, self-consistent sample of planet properties (Zhou et al. 2019; Yee et al. 2021).

There is an obvious trend in the eccentricity distribution of giant planets, where long period giant planets tend to have a wider distribution of orbital eccentricities then shorter period systems, possibly indicative of the system's migration history. If a planet migrates to a close-in configuration through dynamical interactions with other bodies, it can result in a highly eccentric and/or misaligned orbit (Rasio & Ford 1996; Wu & Lithwick 2011). Specifically, looking at Figure 6, we see that the eccentricity range appears to broaden beyond an orbital period of ∼3 days. We note that many components of a planet's formation and evolutionary history are incorporated in this distribution, and a proper analysis of the population as a function of host star parameters is warranted prior to drawing any conclusions. This trend is also seen for brown dwarfs, indicating that more massive systems may undergo migration scenarios similar to planets (Carmichael et al. 2021).

Another possible piece of the puzzle is that a tentative trend has emerged where longer period hot Jupiters (>5 days) are more massive than shorter period ones (Ikwut-Ukwa et al. 2022). Unfortunately, the lack of homogenity of the current exoplanet population makes any observed trends difficult to interpret since they may only manifest due to the different assumptions and analysis techniques used. More importantly, Figure 6 shows the large impact *TESS* is making on the field of giant planets purely from the large number of Jovian-sized planets it has discovered to date, with many of them on longer orbital periods (P > 5 days) where the ground-based transit surveys struggled due to poor duty cycles (Gaudi et al. 2005). With the expectation of hundreds of additional discoveries as *TESS* continues to scan the entire sky, the community will have a large number of systems to consider for future detailed characterization using ongoing

[9] https://exoplanetarchive.ipac.caltech.edu, accessed April 2022

Table 6. Median values and 68% confidence intervals for the global models

Priors:		TOI-1811 b	TOI-2025 b	TOI-2145 b	TOI-2152A b	TOI-2154 b	TOI-2497 b
Gaussian	π Gaia Parallax (mas)	7.800±0.051	2.9775±0.0312	4.4509±0.0314	3.3018±0.0417	3.3744±0.0337	3.5072±0.0508
Gaussian	[Fe/H] Metallicity (dex)	0.27±0.08	0.19±0.08	0.23±0.08	0.27±0.08	0.02±0.08	0.06±0.08
Upper Limit	A_V V-band extinction (mag)	0.04619	0.1801	0.1004	2.0150	0.2793	1.3020
Gaussian	T_C^{**} Time of conjunction (HJD_{TDB})	2454006.04900±0.00337	—	—	—	—	—
Gaussian′	D_T Dilution in *TESS*	0.00000±0.00028	0.00000±0.00026	—	0.00000±0.02032	0.00000±0.00055	—
Parameter	Units	Values	Values	Values	Values	Values	Values
Stellar Parameters:							
M_*	Mass ($M_\odot$)	$0.819^{+0.033}_{-0.030}$	$1.176^{+0.079}_{-0.091}$	$1.720^{+0.057}_{-0.068}$	$1.516^{+0.085}_{-0.10}$	$1.233^{+0.077}_{-0.090}$	$1.861^{+0.086}_{-0.081}$
R_*	Radius ($R_\odot$)	$0.773^{+0.019}_{-0.017}$	$1.489^{+0.040}_{-0.039}$	$2.738^{+0.065}_{-0.064}$	$1.612^{+0.056}_{-0.051}$	$1.396^{+0.049}_{-0.043}$	$2.358^{+0.085}_{-0.082}$
L_*	Luminosity ($L_\odot$)	$0.2749^{+0.0071}_{-0.0070}$	$2.47^{+0.12}_{-0.11}$	$9.92^{+0.32}_{-0.34}$	$4.50^{+0.77}_{-0.64}$	$2.72^{+0.23}_{-0.20}$	$14.7^{+2.0}_{-1.7}$
F_{Bol}	Bolometric Flux $\times 10^{-9}$ (cgs)	0.535 ± 0.012	$0.698^{+0.031}_{-0.029}$	$6.29^{+0.18}_{-0.20}$	$1.57^{+0.26}_{-0.22}$	$0.992^{+0.080}_{-0.071}$	$5.80^{+0.76}_{-0.63}$
ρ_*	Density (g cm^{-2})	$2.51^{+0.18}_{-0.19}$	$0.500^{+0.057}_{-0.054}$	0.1178 ± 0.0091	$0.511^{+0.062}_{-0.066}$	$0.639^{+0.083}_{-0.087}$	$0.200^{+0.027}_{-0.023}$
$\log g$	Surface gravity (cgs)	$4.576^{+0.023}_{-0.025}$	$4.161^{+0.038}_{-0.043}$	$3.798^{+0.023}_{-0.026}$	$4.205^{+0.038}_{-0.048}$	$4.239^{+0.042}_{-0.051}$	$3.963^{+0.040}_{-0.039}$
$T_{\rm eff}$	Effective Temperature (K)	4753^{+54}_{-55}	5928^{+76}_{-75}	6189 ± 67	6630^{+300}_{-290}	6280 ± 160	7360^{+290}_{-270}
[Fe/H]	Metallicity (dex)	$0.320^{+0.075}_{-0.077}$	$0.178^{+0.068}_{-0.069}$	$0.245^{+0.074}_{-0.072}$	$0.282^{+0.075}_{-0.079}$	$0.011^{+0.071}_{-0.059}$	$0.094^{+0.076}_{-0.072}$
$[Fe/H]_0^{\dagger}$	Initial Metallicity	$0.293^{+0.073}_{-0.076}$	0.220 ± 0.062	$0.285^{+0.070}_{-0.067}$	$0.368^{+0.063}_{-0.070}$	$0.105^{+0.059}_{-0.056}$	$0.177^{+0.077}_{-0.073}$
Age	Age (Gyr)	$6.0^{+4.8}_{-4.1}$	$5.4^{+2.7}_{-1.7}$	$1.79^{+0.30}_{-0.23}$	$0.83^{+1.1}_{-0.58}$	$2.9^{+2.1}_{-1.5}$	$1.00^{+0.20}_{-0.18}$
$EEP^{\ddagger}$	Equal Evolutionary Phase	335^{+15}_{-33}	420^{+24}_{-30}	$401.4^{+10.}_{-8.7}$	328^{+22}_{-35}	369^{+46}_{-33}	$360.2^{+11}_{-9.0}$
A_V	V-band extinction (mag)	$0.024^{+0.015}_{-0.016}$	$0.089^{+0.054}_{-0.053}$	$0.071^{+0.021}_{-0.035}$	$0.98^{+0.17}_{-0.18}$	$0.137^{+0.088}_{-0.087}$	0.52 ± 0.12
σ_{SED}	SED photometry error scaling	$0.86^{+0.35}_{-0.21}$	$0.49^{+0.20}_{-0.12}$	$0.92^{+0.33}_{-0.21}$	$1.09^{+0.40}_{-0.25}$	$0.67^{+0.27}_{-0.16}$	$0.70^{+0.28}_{-0.17}$
ϖ	Parallax (mas)	$7.801^{+0.050}_{-0.051}$	2.974 ± 0.031	4.452 ± 0.031	3.302 ± 0.042	3.374 ± 0.034	3.507 ± 0.051
d	Distance (pc)	$128.20^{+0.84}_{-0.82}$	336.3 ± 3.5	224.6 ± 1.6	$302.8^{+3.9}_{-3.8}$	$296.3^{+3.0}_{-2.9}$	$285.1^{+4.2}_{-4.1}$
Planetary Parameters:							
P	Period (days)	3.7130818 ± 0.0000028	$8.8720942^{+0.0000080}_{-0.0000079}$	$10.261081^{+0.000026}_{-0.000027}$	$3.3773512^{+0.0000060}_{-0.0000061}$	3.8240801 ± 0.0000025	10.655661 ± 0.000026
R_P	Radius (R_J)	$1.002^{+0.026}_{-0.024}$	$1.118^{+0.031}_{-0.030}$	$1.103^{+0.031}_{-0.029}$	$1.281^{+0.050}_{-0.046}$	$1.453^{+0.053}_{-0.048}$	$1.000^{+0.040}_{-0.038}$
M_P	Mass (M_J)	$0.974^{+0.075}_{-0.076}$	$3.51^{+0.36}_{-0.35}$	$5.35^{+0.32}_{-0.35}$	$2.83^{+0.38}_{-0.37}$	$0.92^{+0.19}_{-0.18}$	5.21 ± 0.52
T_C	Time of conjunction (BJD_{TDB})	$2458899.87076^{+0.00020}_{-0.00019}$	$2458690.28899^{+0.00046}_{-0.00047}$	$2459013.28046^{+0.00072}_{-0.00071}$	$2458792.55575 \pm 0.00034$	$2458819.73080^{+0.0011}_{-0.00079}$	2459205.0993 ± 0.0011
$T_0^{\star}$	Optimal conjunction Time (BJD_{TDB})	$2459003.83705^{+0.00018}_{-0.00016}$	$2459062.91695^{+0.00032}_{-0.00033}$	$2459208.24100 \pm 0.00050$	$2458927.64980 \pm 0.00023$	$2459148.60166^{+0.0011}_{-0.00072}$	$2458981.33037^{+0.00099}_{-0.00090}$
a	Semi-major axis (AU)	$0.04393^{+0.00058}_{-0.00054}$	$0.0886^{+0.0019}_{-0.0024}$	$0.1108^{+0.0012}_{-0.0015}$	$0.05064^{+0.00093}_{-0.0011}$	$0.0513^{+0.0011}_{-0.0013}$	$0.1167^{+0.0018}_{-0.0017}$
i	Inclination (Degrees)	$86.41^{+0.17}_{-0.21}$	$86.47^{+0.27}_{-0.32}$	$87.41^{+1.4}_{-0.88}$	$86.42^{+1.4}_{-0.85}$	$83.37^{+0.55}_{-0.75}$	$88.11^{+1.1}_{-0.72}$
e	Eccentricity	$0.061^{+0.061}_{-0.042}$	$0.220^{+0.052}_{-0.053}$	$0.182^{+0.039}_{-0.049}$	$0.057^{+0.068}_{-0.040}$	$0.117^{+0.10}_{-0.079}$	$0.196^{+0.059}_{-0.053}$
$\tau_{\rm circ}^{\pi}$	Tidal circularization timescale (Gyr)	0.70 ± 0.14	48^{+22}_{-16}	232^{+57}_{-50}	$0.60^{+0.18}_{-0.17}$	$0.129^{+0.061}_{-0.050}$	430^{+160}_{-140}
ω_*	Argument of Periastron (Degrees)	25^{+51}_{-30}	94^{+19}_{-18}	$100.3^{+10.}_{-9.6}$	96^{+83}_{-89}	31^{+98}_{-36}	-22^{+20}_{-19}
T_{eq}	Equilibrium temperature (K)	961.5 ± 8.0	1172^{+18}_{-17}	1484^{+16}_{-14}	1802^{+60}_{-54}	1580 ± 27	1596^{+44}_{-41}
K	RV semi-amplitude (m/s)	146 ± 11	318^{+29}_{-30}	354^{+19}_{-21}	291 ± 36	105 ± 21	324 ± 31
R_P/R_*	Radius of planet in stellar radii	$0.13316^{+0.00088}_{-0.00085}$	$0.07713^{+0.00067}_{-0.00068}$	$0.04140^{+0.00041}_{-0.00036}$	0.0816 ± 0.0012	$0.10693^{+0.00095}_{-0.00090}$	$0.04355^{+0.00057}_{-0.00049}$
a/R_*	Semi-major axis in stellar radii	$12.23^{+0.29}_{-0.32}$	$12.78^{+0.47}_{-0.48}$	$8.70^{+0.22}_{-0.23}$	$6.76^{+0.26}_{-0.31}$	$7.91^{+0.33}_{-0.37}$	$10.64^{+0.45}_{-0.42}$
Depth	Flux decrement at mid transit	$0.01773^{+0.00024}_{-0.00023}$	0.00595 ± 0.00010	$0.001714^{+0.000034}_{-0.000030}$	$0.00666^{+0.00020}_{-0.00019}$	$0.01143^{+0.00020}_{-0.00019}$	$0.001896^{+0.000050}_{-0.000043}$
$Depth_{\rm TESS}$	Flux decrement at mid transit for *TESS*	0.01804 ± 0.00016	0.006396 ± 0.000068	0.001900 ± 0.000029	$0.00728^{+0.00018}_{-0.00017}$	$0.01046^{+0.00015}_{-0.00014}$	0.002028 ± 0.000040
τ	Ingress/egress transit duration (days)	$0.01936^{+0.00089}_{-0.00083}$	$0.0178^{+0.0016}_{-0.0015}$	$0.0138^{+0.0018}_{-0.0013}$	0.0140 ± 0.0019	$0.0345^{+0.0023}_{-0.0022}$	$0.0157^{+0.0034}_{-0.0019}$
T_{14}	Total transit duration (days)	0.08070 ± 0.00064	0.1575 ± 0.0014	$0.3114^{+0.0021}_{-0.0017}$	$0.1548^{+0.0017}_{-0.0016}$	0.1027 ± 0.0010	$0.3284^{+0.0034}_{-0.0026}$
b	Transit Impact parameter	$0.744^{+0.011}_{-0.012}$	$0.625^{+0.036}_{-0.042}$	$0.32^{+0.13}_{-0.18}$	$0.415^{+0.098}_{-0.18}$	$0.8636^{+0.0071}_{-0.0082}$	$0.36^{+0.16}_{-0.22}$
$T_{S,14}$	Total eclipse duration (days)	$0.08110^{+0.00060}_{-0.00072}$	$0.142^{+0.017}_{-0.040}$	$0.419^{+0.051}_{-0.047}$	$0.1606^{+0.023}_{-0.0089}$	$0.0965^{+0.0072}_{-0.024}$	$0.290^{+0.033}_{-0.031}$
ρ_P	Density (cgs)	$1.20^{+0.13}_{-0.12}$	$3.11^{+0.44}_{-0.39}$	$4.93^{+0.51}_{-0.50}$	$1.67^{+0.31}_{-0.29}$	$0.370^{+0.092}_{-0.081}$	$6.45^{+1.1}_{-0.98}$
$logg_P$	Surface gravity	$3.381^{+0.038}_{-0.041}$	$3.842^{+0.050}_{-0.052}$	$4.037^{+0.034}_{-0.038}$	$3.630^{+0.065}_{-0.072}$	$3.032^{+0.088}_{-0.10}$	$4.111^{+0.055}_{-0.059}$
T_S	Time of secondary eclipse (BJD_{TDB})	$2458898.12^{+0.16}_{-0.10}$	$2458694.63^{+0.37}_{-0.39}$	$2459018.20^{+0.19}_{-0.20}$	$2458794.241^{+0.084}_{-0.099}$	$2458817.94^{+0.37}_{-0.23}$	$2459200.93^{+0.27}_{-0.29}$
$e\cos\omega_*$		$0.043^{+0.069}_{-0.043}$	$-0.017^{+0.064}_{-0.067}$	$-0.031^{+0.029}_{-0.030}$	$-0.002^{+0.039}_{-0.046}$	$0.051^{+0.15}_{-0.094}$	$0.171^{+0.040}_{-0.042}$
$e\sin\omega_*$		$0.022^{+0.032}_{-0.024}$	$0.207^{+0.052}_{-0.053}$	$0.177^{+0.039}_{-0.050}$	$0.022^{+0.076}_{-0.039}$	$0.035^{+0.054}_{-0.042}$	$-0.071^{+0.065}_{-0.085}$
d/R_*	Separation at mid transit	$11.90^{+0.59}_{-0.69}$	$10.07^{+1.0}_{-0.95}$	$7.16^{+0.50}_{-0.44}$	$6.58^{+0.48}_{-0.68}$	$7.48^{+0.69}_{-0.77}$	$11.09^{+1.0}_{-0.92}$

NOTES:

See Table 3 in Eastman et al. (2019) for a detailed description of all derived and fitted parameters.

$^{**}T_C$ prior comes from analysis of the WASP photometry (see §2.3). We note that this time is in HJD_{TDB} while all data files and results here are BJD_{TDB}. The difference between these two time systems is on the order of seconds while the precision on T_C used as a prior is on order of minutes, and therefore has no influence on the results.

′We assume the TESS correction for blending is much better than 10%. We use a prior of 10% of the determined blending from TICv8 (Stassun et al. 2018).

†The initial metallicity is the metallicity of the star when it was formed.

‡The Equal Evolutionary Point corresponds to static points in a stars evolutionary history when using the MIST isochrones and can be a proxy for age. See §2 in Dotter (2016) for a more detailed description of EEP.

⋆Optimal time of conjunction minimizes the covariance between T_C and Period. This is the transit mid-point.

$^{\pi}$The tidal quality factor (Q_S) is assumed to be 10^6.

and future facilities like the James Webb Space Telescope (JWST), the Atmospheric Remote-sensing Infrared Exoplanet Large-survey (ARIEL, Tinetti et al. 2016), and future 30-meter class ground-based telescopes. Future work should consider obtaining Doppler spectroscopy on TOI-2497 b to determine the orbital obliquity of the planet, a key aspect related to a planet's migration history.

5 CONCLUSION

Using a combination of photometric and spectroscopic observations, we present the discovery of six new hot and warm giant planets (TOI-1811 b, TOI-2025 b, TOI-2145 b, TOI-2152A b, TOI-2154 b, and TOI-2497 b). These systems increase the number of giant planets discovered by *TESS* to date and are a part of a larger effort to

Table 7. Median values and 68% confidence intervals for the global models

TOI-1811						
Wavelength Parameters:		B	R	g'	i'	r'
z'	TESS	V				
u_1	linear limb-darkening coeff	$0.945^{+0.036}_{-0.037}$	$0.655^{+0.046}_{-0.047}$	$0.928^{+0.047}_{-0.049}$	0.486 ± 0.023	$0.698^{+0.045}_{-0.046}$
0.428 ± 0.035	0.403 ± 0.040	0.747 ± 0.050				
u_2	quadratic limb-darkening coeff	-0.114 ± 0.037	$0.191^{+0.047}_{-0.048}$	$-0.031^{+0.048}_{-0.049}$	0.172 ± 0.022	0.146 ± 0.047
$0.222^{+0.035}_{-0.034}$	0.106 ± 0.044	0.050 ± 0.050				
A_D	Dilution from neighboring stars	—	—	—	—	—
–	-0.00000 ± 0.00028	—				
Telescope Parameters:		TRES				
γ_{rel}	Relative RV Offset (m/s)	$-187.2^{+9.1}_{-9.7}$				
σ_J	RV Jitter (m/s)	17^{+14}_{-17}				
σ_J^2	RV Jitter Variance	300^{+660}_{-320}				
Transit Parameters:		TESS UT 2020-01-S2 (TESS)	LCOHAL0m4 UT 2020-04-23 (i')	LCOSSO0m4 UT 2020-04-23 (i')	BYU UT 2020-04-27 (R)	ULMT UT 2020-04-27 (i')
Montcabrer UT 2020-04-30 (i')	BYU12in UT 2020-05-08 (V)	ElSauce UT 2020-05-12 (B)	LCOSSO1m UT 2021-02-25 (B)	LCOSSO1m UT 2021-02-25 (z')	MUSCAT2 UT 2021-06-05 (g')	MUSCAT2 UT 2021-06-05 (i')
MUSCAT2 UT 2021-06-05 (r')	MUSCAT2 UT 2021-06-05 (z')					
σ^2	Added Variance$\times 10^{-5}$	0.040 ± 0.016	$5.83^{+1.2}_{-1.00}$	$1.10^{+0.61}_{-0.49}$	$0.076^{+0.066}_{-0.056}$	$0.101^{+0.034}_{-0.028}$
$0.35^{+0.19}_{-0.16}$	$2.09^{+0.40}_{-0.33}$	$1.20^{+0.53}_{-0.42}$	$0.24^{+0.14}_{-0.11}$	$1.16^{+0.30}_{-0.24}$	$-14.29^{+0.40}_{-0.35}$	$-1.824^{+0.089}_{-0.080}$
$-7.92^{+0.12}_{-0.11}$	$-3.94^{+0.23}_{-0.20}$					
F_0	Baseline flux	1.000026 ± 0.000060	$1.00228^{+0.00082}_{-0.00079}$	$1.01012^{+0.00067}_{-0.00066}$	$1.00004^{+0.00022}_{-0.00021}$	$0.99875^{+0.00016}_{-0.00017}$
$1.00850^{+0.00034}_{-0.00035}$	1.00029 ± 0.00047	0.99766 ± 0.00061	0.99519 ± 0.00035	0.99926 ± 0.00049	1.01265 ± 0.00043	1.01004 ± 0.00023
1.01186 ± 0.00024	1.01135 ± 0.00034					
C_0	Additive detrending coeff	—	0.0074 ± 0.0023	-0.0037 ± 0.0022	0.00380 ± 0.00052	$0.00516^{+0.00042}_{-0.00041}$
$0.00187^{+0.00061}_{-0.00064}$	-0.0039 ± 0.0012	$0.0053^{+0.0019}_{-0.0018}$	$0.00822^{+0.00091}_{-0.00089}$	0.0012 ± 0.0013	-0.02691 ± 0.00090	$-0.01075^{+0.00048}_{-0.00047}$
-0.01899 ± 0.00047	$-0.00612^{+0.00094}_{-0.00095}$					
TOI-2025						
Wavelength Parameters:		B	Kepler	R	g'	i'
TESS	V					
u_1	linear limb-darkening coeff	$0.629^{+0.052}_{-0.053}$	0.401 ± 0.038	$0.351^{+0.051}_{-0.050}$	0.565 ± 0.053	0.287 ± 0.037
$0.283^{+0.026}_{-0.027}$	$0.448^{+0.038}_{-0.039}$					
u_2	quadratic limb-darkening coeff	$0.169^{+0.052}_{-0.051}$	$0.302^{+0.036}_{-0.035}$	0.297 ± 0.049	$0.229^{+0.051}_{-0.052}$	0.292 ± 0.036
0.282 ± 0.027	0.274 ± 0.036					
A_D	Dilution from neighboring stars	–	–	–	–	–
0.00001 ± 0.00025	–					
Telescope Parameters:		TRES				
γ_{rel}	Relative RV Offset (m/s)	180 ± 22				
σ_J	RV Jitter (m/s)	74^{+26}_{-19}				
σ_J^2	RV Jitter Variance	5600^{+4600}_{-2500}				
Transit Parameters:		TESS UT 2019-al-l. (TESS)	LCOTFN UT 2020-06-26 (g')	LCOTFN UT 2020-06-26 (i')	SCT UT 2020-06-26 (TESS)	TESS UT 2021-01-01 (TESS)
KeplerCam UT 2021-05-12 (B)	KeplerCam UT 2021-05-12 (i')	GMU UT 2021-05-20 (V)	CRCAO UT 2021-05-21 (R)	MORP UT 2021-09-30 (Kepler)	MORP UT 2021-10-18 (Kepler)	Conti UT 2021-12-19 (V)
σ^2	Added Variance$\times 10^{-5}$	$-0.0058^{+0.0013}_{-0.0012}$	$1.07^{+0.31}_{-0.25}$	$1.07^{+0.29}_{-0.24}$	$2.65^{+0.24}_{-0.22}$	$-0.0022^{+0.010}_{-0.0099}$
$0.525^{+0.065}_{-0.056}$	$1.34^{+0.16}_{-0.14}$	$1.27^{+0.28}_{-0.24}$	$0.396^{+0.069}_{-0.060}$	$0.551^{+0.055}_{-0.049}$	$0.389^{+0.049}_{-0.045}$	$1.78^{+0.33}_{-0.31}$
F_0	Baseline flux	1.000001 ± 0.000022	0.99929 ± 0.00045	0.99950 ± 0.00044	0.99978 ± 0.00028	1.000891 ± 0.000042
1.00360 ± 0.00019	1.00375 ± 0.00029	1.00040 ± 0.00038	1.00380 ± 0.00019	1.00016 ± 0.00014	0.99791 ± 0.00012	1.00283 ± 0.00029
C_0	Additive detrending coeff	–	0.00250 ± 0.00096	0.00138 ± 0.00093	-0.00066 ± 0.00080	–
$-0.00325^{+0.00043}_{-0.00044}$	-0.00203 ± 0.00067	$-0.00027^{+0.00088}_{-0.00089}$	0.00360 ± 0.00041	–	–	$-0.00571^{+0.00085}_{-0.00086}$
TOI-2145						
Wavelength Parameters:		i'	r'	TESS		
u_1	linear limb-darkening coeff	0.242 ± 0.051	$0.316^{+0.051}_{-0.050}$	0.220 ± 0.029		
u_2	quadratic limb-darkening coeff	0.314 ± 0.050	0.310 ± 0.050	$0.297^{+0.034}_{-0.033}$		
Telescope Parameters:		MINERVAT1	MINERVAT2	MINERVAT3	TRES	
γ_{rel}	Relative RV Offset (m/s)	61 ± 41	-13^{+27}_{-25}	-50^{+140}_{-180}	-194 ± 16	
σ_J	RV Jitter (m/s)	167^{+43}_{-35}	71^{+32}_{-27}	220^{+410}_{-220}	35 ± 22	
σ_J^2	RV Jitter Variance	28000^{+16000}_{-11000}	5100^{+5600}_{-3100}	$47000^{+340000}_{-55000}$	1300^{+2100}_{-1100}	
Transit Parameters:		TESS UT 2020-S2-6S (TESS)	TESS UT 2020-S4-0S (TESS)	ULMoore UT 2021-09-07 (i')	CRCAO UT 2021-09-07 (r')	
σ^2	Added Variance$\times 10^{-5}$	$0.00435^{+0.00087}_{-0.0083}$	$0.00273^{+0.00075}_{-0.00073}$	$1.74^{+0.23}_{-0.20}$	$1.221^{+0.092}_{-0.084}$	
F_0	Baseline flux	1.000900 ± 0.000012	1.000627 ± 0.000011	1.00087 ± 0.00036	1.00066 ± 0.00017	
C_0	Additive detrending coeff	–	–	$-0.00136^{+0.00070}_{-0.00071}$	-0.00398 ± 0.00040	

Table 8. Median values and 68% confidence intervals for the global models

TOI-2152								
Wavelength Parameters:		B	R	g'	i'	TESS		
u_1	linear limb-darkening coeff	$0.484^{+0.067}_{-0.061}$	$0.262^{+0.047}_{-0.044}$	$0.423^{+0.067}_{-0.064}$	$0.207^{+0.057}_{-0.056}$	$0.205^{+0.039}_{-0.040}$		
u_2	quadratic limb-darkening coeff	$0.265^{+0.051}_{-0.054}$	0.337 ± 0.037	$0.287^{+0.056}_{-0.057}$	0.327 ± 0.050	0.330 ± 0.049		
A_D	Dilution from neighboring stars	–	–	–	–	-0.001 ± 0.018		
Telescope Parameters:		TRES						
γ_{rel}	Relative RV Offset (m/s)	207^{+29}_{-28}						
σ_J	RV Jitter (m/s)	83^{+37}_{-26}						
σ_J^2	RV Jitter Variance	7000^{+7500}_{-3700}						
Transit Parameters:		TESS UT 2019-al-l. (TESS)	OWL UT 2020-08-17 (R)	WaffelowCreek UT 2020-10-11 (g')	WaffelowCreek UT 2020-10-11 (i')	CALOU UT 2020-11-24 (B)	Kourovka UT 2020-12-10 (B)	CRCAO UT 2021-06-28 (R)
σ^2	Added Variance $\times 10^{-5}$	$-0.00131^{+0.00098}_{-0.00092}$	$1.16^{+0.21}_{-0.19}$	$0.56^{+0.22}_{-0.18}$	$0.68^{+0.18}_{-0.15}$	$0.73^{+0.20}_{-0.17}$	$0.67^{+0.15}_{-0.12}$	$1.23^{+0.15}_{-0.13}$
F_0	Baseline flux	1.000023 ± 0.000017	1.00036 ± 0.00030	1.00344 ± 0.00038	1.00342 ± 0.00035	$0.99928^{+0.00035}_{-0.00034}$	1.00137 ± 0.00032	1.00032 ± 0.00028
C_0	Additive detrending coeff	–	0.00283 ± 0.00066	$-0.00219^{+0.00094}_{-0.00093}$	$-0.00104^{+0.00084}_{-0.00085}$	0.00109 ± 0.00070	$-0.00132^{+0.00052}_{-0.00051}$	0.00008 ± 0.00044

TOI-2154							
Wavelength Parameters:		B	I	Kepler	z'	TESS	
u_1	linear limb-darkening coeff	0.493 ± 0.056	0.211 ± 0.052	0.325 ± 0.052	0.195 ± 0.038	0.264 ± 0.049	
u_2	quadratic limb-darkening coeff	0.205 ± 0.054	0.298 ± 0.050	$0.306^{+0.049}_{-0.050}$	0.304 ± 0.035	0.329 ± 0.048	
A_D	Dilution from neighboring stars	–	–	–	–	0.00001 ± 0.00055	
Telescope Parameters:		tres					
γ_{rel}	Relative RV Offset (m/s)	10^{+20}_{-18}					
σ_J	RV Jitter (m/s)	32^{+26}_{-32}					
σ_J^2	RV Jitter Variance	1000^{+2300}_{-1100}					
Transit Parameters:		TESS UT 2019-al-l. (TESS)	V390m4 UT 2020-08-18 (I)	OPM UT 2020-10-29 (z')	CALOU UT 2020-11-23 (B)	LCO McD UT 2020-12-03 (z')	MSU UT 2021-10-24 (Kepler)
σ^2	Added Variance $\times 10^{-5}$	$-0.1708^{+0.0014}_{-0.0013}$	$2.42^{+0.59}_{-0.48}$	$1.6^{+1.8}_{-0.000014}$	$0.46^{+0.13}_{-0.11}$	$0.78^{+0.16}_{-0.13}$	$0.139^{+0.044}_{-0.036}$
F_0	Baseline flux	1.000067 ± 0.000021	0.99986 ± 0.00064	0.9959 ± 0.0012	$0.99915^{+0.00027}_{-0.00028}$	1.00037 ± 0.00033	$0.99992^{+0.00018}_{-0.00017}$
C_0	Additive detrending coeff	–	0.0004 ± 0.0011	0.0010 ± 0.0022	–	0.00116 ± 0.00078	0.00064 ± 0.00041
M_0	Multiplicative detrending coeff	–	–	–	0.00160 ± 0.00054	–	–

TOI-2497							
Wavelength Parameters:		TESS					
u_1	linear limb-darkening coeff	0.152 ± 0.034					
u_2	quadratic limb-darkening coeff	$0.326^{+0.035}_{-0.036}$					
Telescope Parameters:		CHIRON	MINERVAT3	MINERVAT4	MINERVAT5	MINERVAT6	TRES
γ_{rel}	Relative RV Offset (m/s)	-28751^{+60}_{-63}	55865^{+82}_{-77}	56050^{+110}_{-100}	56300^{+110}_{-100}	56157^{+74}_{-83}	-346 ± 27
σ_J	RV Jitter (m/s)	151^{+87}_{-61}	205^{+84}_{-69}	260^{+130}_{-100}	100^{+200}_{-100}	59^{+190}_{-59}	83^{+33}_{-28}
σ_J^2	RV Jitter Variance	23000^{+34000}_{-15000}	42000^{+42000}_{-24000}	68000^{+82000}_{-42000}	10000^{+80000}_{-36000}	4000^{+61000}_{-31000}	6900^{+6600}_{-3800}
Transit Parameters:		TESS UT 2018-01-.T (TESS)	TESS UT 2021-01-.T (TESS)				
σ^2	Added Variance $\times 10^{-5}$	$-0.00537^{+0.00062}_{-0.00052}$	0.0018 ± 0.016				
F_0	Baseline flux	$1.000001^{+0.000019}_{-0.000020}$	1.000266 ± 0.000019				

create a complete sample of systems brighter than $G < 12.5$ in support of future population studies. Of the six systems presented here, we note a few interesting aspects. First, TOI-2145 is a bright (G = 8.94±0.02 mag), sub-giant ($\log g$ = $3.798^{+0.023}_{-0.026}$ cgs) with a 10.26 day period and a $\sim$5 M_J planet. Interestingly, we see no signs of inflation from the measured radius of TOI-2145 b, but it is important to note that hot Jupiters discovered around evolved stars suggest planets may re-inflate in the post-main sequence phase (Almenara et al. 2015; Grunblatt et al. 2016; Hartman & Bakos 2016; Stevens et al. 2017; Komacek et al. 2020), when a warm Jupiter (like TOI-2145 b) will receive a similar amount of irradiation to that of a hot Jupiter (Lopez & Fortney 2016). TOI-2152A b and TOI-2154 b are similar orbital period hot Jupiters that orbit similar hosts but the planets are $2.83^{+0.38}_{-0.37}$ M_J and $0.92^{+0.19}_{-0.18}$ M_J providing a nice opportunity for future comparative studies. TOI-2497 b orbits a massive, early F-star ($T_{eff} = 7360^{+290}_{-270}$), and the combination of its host star's brightness (G = 9.47±0.02 mag) and rotation period ($v \sin I_* = 39.6 \pm 1.0$ km s^{-1}) make it well-suited for orbital obliquity measurements through transit spectroscopy followup. *TESS* continues to discover a wealth of

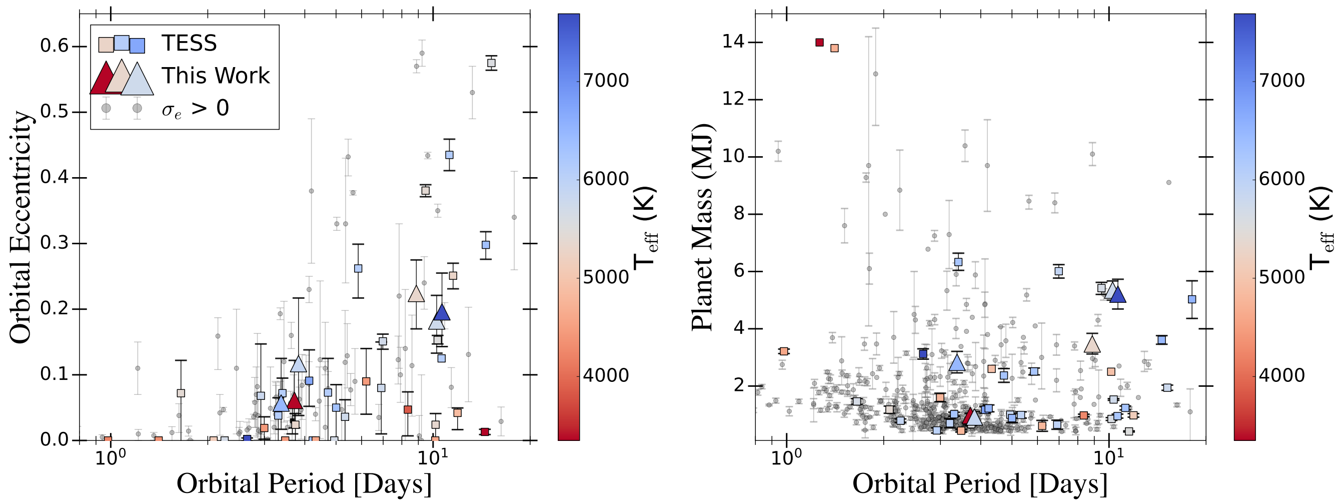

Figure 6. (Left) The eccentricity and log of the orbital period of all known giant planets with a mass greater than 0.4 $M_J$with period between 0.8 and 30 days. The systems with a measured eccentricity from the NASA Exoplanet Archive (NEA) are shown as grey circles with errors. (Right) The mass and log of the orbital period of all known transiting giant planets. In both figures the *TESS* discovered systems (including the ones presented in this work) are the squares colored by the host star's effective temperature (with those from this work are displayed with a triangle symbol).

transiting giant planets that may provide insight into their formation and evolutionary mechanisms.

ACKNOWLEDGEMENTS

L.C, K.S., E.A., J.R., J.E.R., J.A.R., P.W., and E.Z. are grateful for support from NSF grants AST-1751874 and AST-1907790, along with a Cottrell Fellowship from the Research Corporation. CZ is supported by a Dunlap Fellowship at the Dunlap Institute for Astronomy & Astrophysics, funded through an endowment established by the Dunlap family and the University of Toronto. T.H. acknowledges support from the European Research Council under the Horizon 2020 Framework Program via the ERC Advanced Grant Origins 83 24 28. J.V.S. acknowledges funding from the European Research Council (ERC) under the European Union's Horizon 2020 research and innovation programme (project Four Aces; grant agreement No. 724427). P. R. acknowledges support from NSF grant No. 1952545. R.B. acknowledges support from FONDECYT Project 11200751 and from CORFO project N°14ENI2-26865. A.J. R.B. and M.H. acknowledge support from project IC120009 "Millennium Institute of Astrophysics (MAS)" of the Millenium Science Initiative, Chilean Ministry of Economy. D.J.S. acknowledges funding support from the Eberly Research Fellowship from The Pennsylvania State University Eberly College of Science. The Center for Exoplanets and Habitable Worlds is supported by the Pennsylvania State University, the Eberly College of Science, and the Pennsylvania Space Grant Consortium. K.K.M. gratefully acknowledges support from the New York Community Trust's Fund for Astrophysical Research. L.G. and A.G. are supported by NASA Massachusetts Space Grant Fellowships. E.W.G., M.E., and P.C. acknowledge support by Deutsche Forschungsgemeinschaft (DFG) grant HA 3279/12-1 within the DFG Schwerpunkt SPP1992, Exploring the Diversity of Extrasolar Planets. B.S.G. was partially supported by the Thomas Jefferson Chair for Space Exploration at the Ohio State University. C.D. acknowledges support from the Hellman Fellows Fund and NASA XRP via grant 80NSSC20K0250. B.S.S., M.V.G. and A.A.B. acknowledge the support of Ministry of Science and Higher Education of the Russian Federation under the grant 075-15-2020-780 (N13.1902.21.0039). B.A. is supported by Australian Research Council Discovery Grant DP180100972.

We thank the CHIRON team members, including Todd Henry, Leonardo Paredes, Hodari James, Azmain Nisak, Rodrigo Hinojosa, Roberto Aviles, Wei-Chun Jao and CTIO staffs, for their work in acquiring RVs with CHIRON at CTIO. This research has made use of SAO/NASA's Astrophysics Data System Bibliographic Services. This research has made use of the SIMBAD database, operated at CDS, Strasbourg, France. This work has made use of data from the European Space Agency (ESA) mission *Gaia* (https://www.cosmos.esa.int/gaia), processed by the *Gaia* Data Processing and Analysis Consortium (DPAC, https://www.cosmos.esa.int/web/gaia/dpac/consortium). Funding for the DPAC has been provided by national institutions, in particular the institutions participating in the *Gaia* Multilateral Agreement. This work makes use of observations from the LCO network. Based in part on observations obtained at the Southern Astrophysical Research (SOAR) telescope, which is a joint project of the Ministério da Ciência, Tecnologia e Inovações (MCTI/LNA) do Brasil, the US National Science Foundation's NOIRLab, the University of North Carolina at Chapel Hill (UNC), and Michigan State University (MSU).

Funding for the *TESS* mission is provided by NASA's Science Mission directorate. We acknowledge the use of public *TESS* Alert data from pipelines at the *TESS* Science Office and at the *TESS* Science Processing Operations Center. This research has made use of the NASA Exoplanet Archive and the Exoplanet Follow-up Observation Program website, which are operated by the California Institute of Technology, under contract with the National Aeronautics and Space Administration under the Exoplanet Exploration Program. This paper includes data collected by the *TESS* mission, which are publicly available from the Mikulski Archive for Space Telescopes (MAST). This paper includes observations obtained under Gemini program GN-2018B-LP-101. Resources supporting this work were provided by the NASA High-End Computing (HEC) Program through the NASA Advanced Supercomputing (NAS) Division at Ames Research Center for the production of the SPOC data products. This publication makes use of The Data & Analysis Center for Exoplanets (DACE), which is a facility based at the University of Geneva (CH) dedicated to extrasolar planets data visualisation, exchange and analysis. DACE is a platform of the Swiss National Centre of Competence in Research (NCCR) PlanetS, federating the Swiss expertise in Exoplanet research. The DACE platform is available at https://dace.unige.ch.

Some of the data presented herein were obtained at the W. M. Keck Observatory, which is operated as a scientific partnership among the California Institute of Technology, the University of California and the National Aeronautics and Space Administration. The Observatory was made possible by the generous financial support of the W. M. Keck Foundation. The authors wish to recognize and acknowledge the very significant cultural role and reverence that the summit of Mauna Kea has always had within the indigenous Hawaiian community. We are most fortunate to have the opportunity to conduct observations from this mountain.

Minerva-Australis is supported by Australian Research Council LIEF Grant LE160100001 (Discovery Grant DP180100972 and DP220100365) Mount Cuba Astronomical Foundation, and institutional partners University of Southern Queensland, UNSW Sydney, MIT, Nanjing University, George Mason University, University of Louisville, University of California Riverside, University of Florida, and The University of Texas at Austin. We respectfully acknowledge the traditional custodians of all lands throughout Australia, and recognise their continued cultural and spiritual connection to the land, waterways, cosmos, and community. We pay our deepest respects to all Elders, ancestors and descendants of the Giabal, Jarowair, and Kambuwal nations, upon whose lands the Minerva-Australis facility at Mt Kent is situated.

Data presented herein were obtained at the MINERVA-Australis from telescope time allocated under the NN-EXPLORE program with support from the National Aeronautics and Space Administration.

MINERVA-North is a collaboration among the Harvard-Smithsonian Center for Astrophysics, The Pennsylvania State University, the University of Montana, the University of Southern Queensland, University of Pennsylvania, and George Mason University. It is made possible by generous contributions from its collaborating institutions and Mt. Cuba Astronomical Foundation, The David & Lucile Packard Foundation, National Aeronautics and Space Administration (EPSCOR grant NNX13AM97A, XRP 80NSSC22K0233), the Australian Research Council (LIEF grant LE140100050), and the National Science Foundation (grants 1516242, 1608203, and 2007811).

This article is based on observations made with the MuSCAT2 instrument, developed by ABC, at Telescopio Carlos Sánchez operated on the island of Tenerife by the IAC in the Spanish Observatorio del Teide. This work is partly financed by the Spanish Ministry of Economics and Competitiveness through grants PGC2018-098153-B-C31.The work of VK was supported by the Ministry of science and higher education of the Russian Federation, topic FEUZ-2020-0038.

This work is partly supported by JSPS KAKENHI Grant Number JP18H05439, JST CREST Grant Number JPMJCR1761. This article is based on observations made with the MuSCAT2 instrument, developed by ABC, at Telescopio Carlos Sánchez operated on the island of Tenerife by the IAC in the Spanish Observatorio del Teide.

The Center for Exoplanets and Habitable Worlds and the Penn State Extraterrestrial Intelligence Center are supported by Penn State and the Eberly College of Science.

This paper was partially based on observations obtained at the OWL-Net system, which is operated by the Korea Astronomy and Space Science Institute (KASI).

DATA AVAILABILITY

The *TESS* observations used in this paper (see §2.1) and are shown in in Figure 1 are publicly available on the MAST[10] archive. The photometric transit follow up observations from the SG1 working groups in TFOP (underlying data for Figure 3 and 4) are publicly available on Exofop[11], along with the the AO and SPECKLE contrast curves and images discussed in §2.6. The RV data (sample shown in Table 3) underlying this article (shown in Figure 5) are available in the article and in its online supplementary material.

Software Used: `EXOFASTv2` (Eastman et al. 2013, 2019), AstroImageJ (Collins et al. 2017), TAPIR (Jensen 2013), QLP Pipeline (Huang et al. 2020)

Facilities: *TESS*, FLWO 1.5m (Tillinghast Reflector Echelle Spectrograph), 4.1-m Southern Astrophysical Research (SOAR), LCO 0.4m, LCO 1.0m, 2.2m telescope La Silla (Fiber-fed Extended Range Optical Spectrograph), KECK (NIRC2), PALOMAR (PHARO), KELT, WASP, CTIO 1.5m (CHIRON), MINERVA-North,Minerva-Australis, GEMINI (NIRI), CMO 2.5m (SPP)

REFERENCES

Adams F. C., Laughlin G., 2006, ApJ, 649, 1004
Addison B., et al., 2019, PASP, 131, 115003
Addison B. C., et al., 2021, MNRAS, 502, 3704
Almenara J. M., et al., 2015, A&A, 575, A71
Auvergne M., et al., 2009, A&A, 506, 411
Bakos G. Á., et al., 2013, PASP, 125, 154
Barclay T., Pepper J., Quintana E. V., 2018, ApJS, 239, 2
Barros S. C. C., Demangeon O., Deleuil M., 2016, A&A, 594, A100
Borucki W. J., et al., 2010, Science, 327, 977
Boyajian T. S., et al., 2012, ApJ, 757, 112
Bradley L., et al., 2019, astropy/photutils: v0.7.1, doi:10.5281/zenodo.3478575
Brahm R., et al., 2020, AJ, 160, 235
Brasseur C. E., Phillip C., Fleming S. W., Mullally S. E., White R. L., 2019, Astrocut: Tools for creating cutouts of TESS images (ascl:1905.007)
Brown T. M., et al., 2013, PASP, 125, 1031
Buchhave L. A., et al., 2010, ApJ, 720, 1118
Buchhave L. A., et al., 2012, Nature, 486, 375
Burdanov A. Y., Krushinsky V. V., Popov A. A., 2014, Astrophysical Bulletin, 69, 368
Caldwell D. A., et al., 2020, Research Notes of the American Astronomical Society, 4, 201
Cale B., et al., 2019, AJ, 158, 170
Carmichael T. W., et al., 2021, AJ, 161, 97
Castelli F., Hubrig S., 2004, A&A, 425, 263
Choi J., Dotter A., Conroy C., Cantiello M., Paxton B., Johnson B. D., 2016, ApJ, 823, 102
Ciardi D. R., Beichman C. A., Horch E. P., Howell S. B., 2015, ApJ, 805, 16
Collier Cameron A., et al., 2007, MNRAS, 380, 1230
Collins K. A., Kielkopf J. F., Stassun K. G., Hessman F. V., 2017, AJ, 153, 77
Crossfield I. J. M., et al., 2016, ApJS, 226, 7
Cumming A., Butler R. P., Marcy G. W., Vogt S. S., Wright J. T., Fischer D. A., 2008, PASP, 120, 531
Cutri R. M., et al., 2003, VizieR Online Data Catalog, 2246, 0
Cutri R. M., Wright E. L., T. C., at al. 2012, VizieR Online Data Catalog, 2311, 0

[10] https://mast.stsci.edu/
[11] https://exofop.ipac.caltech.edu/tess/

Czesla S., Schröter S., Schneider C. P., Huber K. F., Pfeifer F., Andreasen D. T., Zechmeister M., 2019, PyA: Python astronomy-related packages (ascl:1906.010)
Dawson R. I., Fabrycky D. C., 2010, ApJ, 722, 937
Dawson R. I., Johnson J. A., 2018, Annual Review of Astronomy and Astrophysics, 56, 175
Dekany R., et al., 2013, ApJ, 776, 130
Donati J.-F., Semel M., Carter B. D., Rees D. E., Collier Cameron A., 1997, MNRAS, 291, 658
Dotter A., 2016, ApJS, 222, 8
Eastman J., Gaudi B. S., Agol E., 2013, PASP, 125, 83
Eastman J. D., et al., 2019, arXiv e-prints, p. arXiv:1907.09480
Edwards B., et al., 2021, MNRAS, 504, 5671
Fűrész G., 2008, PhD thesis, University of Szeged, Hungary
Fortney J. J., Dawson R. I., Komacek T. D., 2021, Journal of Geophysical Research (Planets), 126, e06629
Fressin F., et al., 2013, ApJ, 766, 81
Furlan E., et al., 2017, AJ, 153, 71
Gaia Collaboration et al., 2016, A&A, 595, A2
Gaia Collaboration et al., 2018, A&A, 616, A1
Gaia Collaboration et al., 2021, A&A, 649, A1
Gaudi B. S., Seager S., Mallen-Ornelas G., 2005, ApJ, 623, 472
Gavel D., et al., 2014, in Marchetti E., Close L. M., Vran J.-P., eds, Society of Photo-Optical Instrumentation Engineers (SPIE) Conference Series Vol. 9148, Adaptive Optics Systems IV. p. 914805 (arXiv:1407.8207), doi:10.1117/12.2055256
Gray D. F., 2005, The Observation and Analysis of Stellar Photospheres
Grunblatt S. K., et al., 2016, AJ, 152, 185
Grunblatt S. K., et al., 2022, arXiv e-prints, p. arXiv:2201.04140
Guerrero N. M., et al., 2021, ApJS, 254, 39
Hardegree-Ullman K. K., Zink J. K., Christiansen J. L., Dressing C. D., Ciardi D. R., Schlieder J. E., 2020, ApJS, 247, 28
Hartman J. D., Bakos G. Á., 2016, Astronomy and Computing, 17, 1
Hayward T. L., Brandl B., Pirger B., Blacken C., Gull G. E., Schoenwald J., Houck J. R., 2001, PASP, 113, 105
Henderson C. B., Stassun K. G., 2012, ApJ, 747, 51
Howell S. B., et al., 2014, PASP, 126, 398
Huang C. X., et al., 2020, Research Notes of the American Astronomical Society, 4, 206
Ikwut-Ukwa M., et al., 2020, AJ, 160, 209
Ikwut-Ukwa M., et al., 2022, AJ, 163, 9
Jenkins J. M., 2002, ApJ, 575, 493
Jenkins J. M., et al., 2016, in Software and Cyberinfrastructure for Astronomy IV. p. 99133E, doi:10.1117/12.2233418
Jensen E., 2013, Tapir: A web interface for transit/eclipse observability, Astrophysics Source Code Library (ascl:1306.007)
Johnson M. C., Cochran W. D., Albrecht S., Dodson-Robinson S. E., Winn J. N., Gullikson K., 2014, ApJ, 790, 30
Kane S. R., et al., 2021, PASP, 133, 014402
Knudstrup E., et al., 2022, arXiv e-prints, p. arXiv:2204.13956
Komacek T. D., Thorngren D. P., Lopez E. D., Ginzburg S., 2020, ApJ, 893, 36
Kovács G., Bakos G., Noyes R. W., 2005, MNRAS, 356, 557
Kuhn R. B., et al., 2016, MNRAS, 459, 4281
Kupke R., et al., 2012, in Ellerbroek B. L., Marchetti E., Véran J.-P., eds, Society of Photo-Optical Instrumentation Engineers (SPIE) Conference Series Vol. 8447, Adaptive Optics Systems III. p. 84473G, doi:10.1117/12.926470
Kurucz R. L., 1992, in Barbuy B., Renzini A., eds, IAU Symposium Vol. 149, The Stellar Populations of Galaxies. p. 225
Lindegren L., et al., 2018, A&A, 616, A2
Lomb N. R., 1976, Ap&SS, 39, 447
Lopez E. D., Fortney J. J., 2016, ApJ, 818, 4
Masuda K., Winn J. N., 2017, AJ, 153, 187
Maxted P. F. L., et al., 2011, PASP, 123, 547
Mayo A. W., et al., 2018, AJ, 155, 136
McGurk R., et al., 2014, in Marchetti E., Close L. M., Vran J.-P., eds, Society of Photo-Optical Instrumentation Engineers (SPIE) Conference Series Vol. 9148, Adaptive Optics Systems IV. p. 91483A (arXiv:1407.8205), doi:10.1117/12.2057027
McLaughlin D. B., 1924, ApJ, 60
Miller G. R. M., et al., 2010, A&A, 523, A52
Moe M., Kratter K. M., 2021, MNRAS, 507, 3593
Mugrauer M., Michel K.-U., 2020, Astronomische Nachrichten, 341, 996
Mugrauer M., Michel K.-U., 2021, Astronomische Nachrichten, 342, 840
Narita N., et al., 2019, Journal of Astronomical Telescopes, Instruments, and Systems, 5, 015001
Nelson B. E., Ford E. B., Rasio F. A., 2017, AJ, 154, 106
Nielsen L. D., et al., 2019, A&A, 623, A100
Oelkers R. J., et al., 2018, AJ, 155, 39
Paredes L. A., Henry T. J., Quinn S. N., Gies D. R., Hinojosa-Goñi R., James H.-S., Jao W.-C., White R. J., 2021, AJ, 162, 176
Parviainen H., et al., 2019, A&A, 630, A89
Paxton B., Bildsten L., Dotter A., Herwig F., Lesaffre P., Timmes F., 2011, ApJS, 192, 3
Paxton B., et al., 2013, ApJS, 208, 4
Paxton B., et al., 2015, ApJS, 220, 15
Pecaut M. J., Mamajek E. E., 2013a, ApJS, 208, 9
Pecaut M. J., Mamajek E. E., 2013b, ApJS, 208, 9
Pepper J., et al., 2007, PASP, 119, 923
Pepper J., Kuhn R. B., Siverd R., James D., Stassun K., 2012, PASP, 124, 230
Pepper J., Stassun K. G., Gaudi B. S., 2018, KELT: The Kilodegree Extremely Little Telescope, a Survey for Exoplanets Transiting Bright, Hot Stars. p. 128, doi:10.1007/978-3-319-55333-7_128
Petigura E. A., et al., 2018, AJ, 155, 89
Pollacco D. L., et al., 2006, PASP, 118, 1407
Quinn S. N., et al., 2012, ApJ, 756, L33
Rasio F. A., Ford E. B., 1996, Science, 274, 954
Ricker G. R., et al., 2015, Journal of Astronomical Telescopes, Instruments, and Systems, 1, 014003
Rodriguez J. E., et al., 2019, AJ, 157, 191
Rodriguez J. E., et al., 2021, AJ, 161, 194
Rossiter R. A., 1924, ApJ, 60
Safonov B. S., Lysenko P. A., Dodin A. V., 2017, Astronomy Letters, 43, 344
Savel A. B., Dressing C. D., Hirsch L. A., Ciardi D. R., Fleming J. P. C., Giacalone S. A., Mayo A. W., Christiansen J. L., 2020, AJ, 160, 287
Scargle J. D., 1982, ApJ, 263, 835
Schlafly E. F., Finkbeiner D. P., 2011, ApJ, 737, 103
Schlegel D. J., Finkbeiner D. P., Davis M., 1998, ApJ, 500, 525
Shallue C. J., Vanderburg A., 2018, AJ, 155, 94
Siverd R. J., et al., 2012, ApJ, 761, 123
Smith J. C., et al., 2012, PASP, 124, 1000
Stassun K. G., Torres G., 2016, AJ, 152, 180
Stassun K. G., Mathieu R. D., Mazeh T., Vrba F. J., 1999, AJ, 117, 2941
Stassun K. G., et al., 2018, AJ, 156, 102
Stevens D. J., et al., 2017, AJ, 153, 178
Stumpe M. C., Smith J. C., Catanzarite J. H., Van Cleve J. E., Jenkins J. M., Twicken J. D., Girouard F. R., 2014, PASP, 126, 100
Sullivan P. W., et al., 2015, ApJ, 809, 77
Swift J. J., et al., 2015, Journal of Astronomical Telescopes, Instruments, and Systems, 1, 027002
Tinetti G., et al., 2016, in MacEwen H. A., Fazio G. G., Lystrup M., Batalha N., Siegler N., Tong E. C., eds, Society of Photo-Optical Instrumentation Engineers (SPIE) Conference Series Vol. 9904, Space Telescopes and Instrumentation 2016: Optical, Infrared, and Millimeter Wave. p. 99041X, doi:10.1117/12.2232370
Tokovinin A., 2018, PASP, 130, 035002
Tokovinin A., Fischer D. A., Bonati M., Giguere M. J., Moore P., Schwab C., Spronck J. F. P., Szymkowiak A., 2013, PASP, 125, 1336
Torres G., et al., 2007, ApJ, 666, L121
VanderPlas J. T., 2018, ApJS, 236, 16
Vanderburg A., Johnson J. A., 2014, PASP, 126, 948
Vanderburg A., et al., 2016, ApJS, 222, 14
Vanderburg A., et al., 2019, ApJ, 881, L19
Wilson M. L., et al., 2019, arXiv e-prints,

Wright J. T., Marcy G. W., Howard A. W., Johnson J. A., Morton T. D., Fischer D. A., 2012, ApJ, 753, 160
Wu Y., Lithwick Y., 2011, ApJ, 735, 109
Yee S. W., Winn J. N., Hartman J. D., 2021, AJ, 162, 240
Zhou G., et al., 2016, AJ, 152, 136
Zhou G., et al., 2019, AJ, 158, 141
Zhou G., et al., 2020, arXiv e-prints, p. arXiv:2011.13349
Zhou G., et al., 2021, AJ, 161, 2
Ziegler C., et al., 2018, AJ, 155, 161
Ziegler C., Tokovinin A., Briceño C., Mang J., Law N., Mann A. W., 2020, AJ, 159, 19
Zink J. K., et al., 2019, Research Notes of the American Astronomical Society, 3, 43
Zink J. K., et al., 2021, AJ, 162, 259

AFFILIATIONS

[1]Center for Data Intensive and Time Domain Astronomy, Department of Physics and Astronomy, Michigan State University, East Lansing, MI 48824, USA
[2]Center for Astrophysics | Harvard & Smithsonian, 60 Garden St, Cambridge, MA 02138, USA
[3]Department of Physics and Kavli Institute for Astrophysics and Space Research, Massachusetts Institute of Technology, Cambridge, MA 02139, USA
[4]Centre for Astrophysics, University of Southern Queensland, West Street, Toowoomba, QLD 4350, Australia
[5]Caltech IPAC – NASA Exoplanet Science Institute 1200 E. California Ave, Pasadena, CA 91125, USA
[6]Department of Physical Sciences, Kutztown University, Kutztown, PA 19530, USA
[7]George P. and Cynthia Woods Mitchell Institute for Fundamental Physics and Astronomy, Texas A&M University, College Station, TX77843 USA
[8]Charles R. & Judith G. Munnerlyn Astronomical Laboratory, Department of Physics & Astronomy, Texas A&M University, College Station, TX 77843, USA
[9]Center for Gravitational Wave Astronomy, The University of Texas Rio Grande Valley, Brownsville, TX 78520, USA
[10]Department of Astronomy, The Ohio State University, 140 West 18th Avenue, Columbus, OH 43210, USA
[11]Astrophysics Group, Keele University, Staffordshire ST5 5BG, UK
[12]Kotizarovci Observatory, Sarsoni 90, 51216 Viskovo, Croatia
[13]Department of Physics and Astronomy, University of Louisville, Louisville, KY 40292, USA
[14]Observatri de Ca l'Ou
[15]Villa '39 Observatory, Landers, CA 92285, USA
[16]El Sauce Observatory, Coquimbo Province, Chile
[17]Department of Physics and Astronomy, Brigham Young University, Provo, UT 84602, USA
[18]Department of Astronomy, Wellesley College, Wellesley, MA 02481, USA
[19]Ural Federal University, Ekaterinburg, Russia, ul. Mira d. 19, Yekaterinburg, Russia, 620002
[20]Oukaimeden Observatory, High Energy Physics and Astrophysics Laboratory, Cadi Ayyad University, Marrakech, Morocco
[21]Astrobiology Research Unit, Université de Liège, 19C Allée du 6 Août, 4000 Liège, Belgium
[22]Sternberg Astronomical Institute, M.V. Lomonosov Moscow State University, 13, Universitetskij pr., 119234, Moscow, Russia
[23]Department of Astronomy & Astrophysics, The Pennsylvania State University, 525 Davey Lab, University Park, PA 16802, USA
[24]Center for Exoplanets and Habitable Worlds, The Pennsylvania State University, 525 Davey Lab, University Park, PA 16802, USA
[25]American Association of Variable Star Observers, 49 Bay State Road, Cambridge, MA 02138, USA
[26]Department of Astronomy, University of California Berkeley, Berkeley, CA 94720-3411, USA
[27]Department of Physics, Engineering and Astronomy, Stephen F. Austin State University, TX 75962, USA
[28]Observatori Astronômic Albanyà, Camí de Bassegoda S/N, Albanyà 17733, Girona, Spain
[29]Citizen Scientist
[30]Instituto de Astrofísica de Canarias (IAC), E-38205 La Laguna, Tenerife, Spain
[31]Departamento de Astrofísica, Universidad de La Laguna (ULL), E-38206 La Laguna, Tenerife, Spain
[32]Waffelow Creek Observatory
[33]Department of Astrophysical Sciences, Princeton University, 4 Ivy Lane, Princeton, NJ, 08544, USA
[34]NASA Ames Research Center, Moffett Field, CA, 94035, USA
[35]George Mason University, 4400 University Drive MS 3F3, Fairfax, VA 22030, USA
[36]Department of Physics, University of Warwick, Gibbet Hill Road, Coventry CV4 7AL, UK
[37]School of Physics, Sydney Institute for Astronomy (SIfA), The University of Sydney, NSW 2006, Australia
[38]The University of Pennsylvania, Department of Physics and Astronomy, Philadelphia, PA, 19104, USA
[39]Department of Astronomy, The University of Texas at Austin, Austin, TX 78712, USA
[40]Department of Physics and Astronomy, University of Montana, 32 Campus Drive, No. 1080, Missoula, MT 59812 USA
[41]Cerro Tololo Inter-American Observatory, Casilla 603, La Serena, Chile
[42]Department of Physics and Astronomy, University of Utah, 115 South 1400 East, Salt Lake City, UT 84112, USA
[43]Fundamental and Applied Physics Laboratory, Physics Department, Polydisciplinary Faculty of Safi, Cadi Ayyad University, Marrakesh, Morocco
[44]Department of Physics and Astronomy, Vanderbilt University, Nashville, TN 37235, USA
[45]Department of Astronomy, Tsinghua University, Beijing 100084, China
[46]ASTRAVEO, LLC, PO Box 1668, Gloucester, MA 01931
[47]Department of Earth and Planetary Sciences, University of California, Riverside, CA 92521, USA
[48]Department of Earth, Atmospheric and Planetary Sciences, Massachusetts Institute of Technology, Cambridge, MA 02139, USA
[49]Korea Astronomy and Space Science Institute, 776 Daedeokdaero, Yuseong-gu, Daejeon 34055, Republic of Korea
[50]Thomas Jefferson High School, 6560 Braddock Rd, Alexandria, VA 22312 USA
[51]South African Astronomical Observatory, PO Box 9, Observatory, 7935, Cape Town, South Africa
[52]Southern African Large Telescope, PO Box 9, Observatory, 7935, Cape Town, South Africa
[53]Department of Physics and Astronomy, University of North Carolina at Chapel Hill, Chapel Hill, NC 27599, USA
[54]The Maury Lewin Astronomical Observatory, Glendora,California.91741. USA
[55]School of Astronomy and Space Science, Key Laboratory of

Modern Astronomy and Astrophysics in Ministry of Education, Nanjing University, Nanjing 210046, Jiangsu, China
[56]Astrobiology Center, 2-21-1 Osawa, Mitaka, Tokyo 181-8588, Japan
[57]Komaba Institute for Science, The University of Tokyo, 3-8-1 Komaba, Meguro, Tokyo 153-8902, Japan
[58]Physikalisches Institut, University of Bern, Gesellschaftsstrasse 6, 3012 Bern, Switzerland
[59]Department of Physics, Lehigh University, 16 Memorial Drive East, Bethlehem, PA 18015, USA
[60]Departamento de Matemática y Física Aplicadas, Facultad de Ingeniería, Universidad Católica de la Santísima Concepción, Alonso de Rivera 2850, Concepción, Chile
[61]Department of Astronomy, University of Maryland, College Park, College Park, MD
[62]Patashnick Voorheesville Observatory, Voorheesville, NY 12186, USA
[63]Gemini Observatory/NSF's NOIRLab, 670 N. A'ohoku Place, Hilo, HI, 96720, USA
[64]Department of Physics, Fisk University, 1000 17th Avenue North, Nashville, TN 37208, USA
[65]Instituto de Astrofísica e Ciències do Espaço, CAUP, Universidade do Porto, Rua das Estrelas, 4150-762, Porto, Portugal
[66]Departamento de física, e Astronomia, Faculdade de Ciències, Universidade do Porto, Rua Campo Alegre, 4169-007, Porto, Portugal
[67]Exoplanetary Science at UNSW, School of Physics, UNSW Sydney, NSW 2052, Australia
[68]Centre for Exoplanets and Habitability, University of Warwick, Gibbet Hill Road, Coventry CV4 7AL, UK
[69]Penn State Extraterrestrial Intelligence Center, 525 Davey Laboratory, The Pennsylvania State University, University Park, PA, 16802, USA
[70]Shanghai Astronomical Observatory, Chinese Academy of Sciences, Shanghai 200030, China